Solar Phys
DOI 10.1007/s11207-014-0524-8

> 25 MeV Proton Events Observed by the High Energy Telescopes on the STEREO A and B Spacecraft and/or at Earth During the First ∼ Seven Years of the STEREO Mission

I.G. Richardson · T.T. von Rosenvinge · H.V. Cane · E.R. Christian · C.M.S. Cohen · A.W. Labrador · R.A. Leske · R.A. Mewaldt · M.E. Wiedenbeck · E.C. Stone

Received: 27 September 2013 / Accepted: 27 March 2014

Abstract Using observations from the *High Energy Telescopes* (HETs) on the STEREO A and B spacecraft and similar observations from near-Earth spacecraft, we summarize the

I.G. Richardson (✉) · T.T. von Rosenvinge · E.R. Christian
NASA/Goddard Space Flight Center, Greenbelt, MD 20771, USA
e-mail: ian.g.richardson@nasa.gov

T.T. von Rosenvinge
e-mail: tycho.t.vonrosenvinge@nasa.gov

E.R. Christian
e-mail: eric.r.christian@nasa.gov

I.G. Richardson
CRESST and Department of Astronomy, University of Maryland, College Park, MD 20742, USA

H.V. Cane
Bruny Island Radio Spectrometer, Bruny Island, Tasmania, Australia
e-mail: hcane@utas.edu.au

C.M.S. Cohen · A.W. Labrador · R.A. Leske · R.A. Mewaldt · E.C. Stone
California Institute of Technology, Mail Code 290-17, Pasadena, CA 91125, USA

C.M.S. Cohen
e-mail: cohen@srl.caltech.edu

A.W. Labrador
e-mail: labrador@srl.caltech.edu

R.A. Leske
e-mail: ral@srl.caltech.edu

R.A. Mewaldt
e-mail: rmewaldt@srl.caltech.edu

E.C. Stone
e-mail: ecs@srl.caltech.edu

M.E. Wiedenbeck
Jet Propulsion Laboratory, California Institute of Technology, Pasadena, CA 91109, USA
e-mail: mark.e.wiedenbeck@jpl.nasa.gov

Published online: 15 April 2014

properties of more than 200 individual >25 MeV solar proton events, some detected by multiple spacecraft, that occurred from the beginning of the STEREO mission in October 2006 to December 2013, and provide a catalog of these events and their solar sources and associations. Longitudinal dependencies of the electron and proton peak intensities and delays to onset and peak intensity relative to the solar event have been examined for 25 three-spacecraft particle events. Expressed as Gaussians, peak intensities fall off with longitude with $\sigma = 47 \pm 14^{\circ}$ for 0.7 – 4 MeV electrons, and $\sigma = 43 \pm 13^{\circ}$ for 14 – 24 MeV protons. Several particle events are discussed in more detail, including one on 3 November 2011, in which $\sim$25 MeV protons filled the inner heliosphere within 90 minutes of the solar event, and another on 7 March 2012, in which we demonstrate that the first of two coronal mass ejections that erupted from an active region within $\sim$1 hour was associated with particle acceleration. Comparing the current Solar Cycle 24 with the previous cycle, the first >25 MeV proton event was detected at Earth in the current solar cycle around one year after smoothed sunspot minimum, compared with a delay of only two months in Cycle 23. Otherwise, solar energetic particle event occurrence rates were reasonably similar during the rising phases of Cycles 23 and 24. However, the rate declined in 2013, reflecting the decline in sunspot number since the peak in the northern-hemisphere sunspot number in November 2011. Observations in late 2013 suggest that the rate may be rising again in association with an increase in the southern sunspot number.

Keywords Solar energetic particles · STEREO · SOHO

1. Introduction

With the launch of the STEREO A ("*Ahead*") and B ("*Behind*") spacecraft on 26 October 2006 into heliocentric orbits advancing ahead of or lagging Earth in its orbit, respectively, solar energetic particle (SEP) events can be observed at multiple locations near 1 AU. Even when closely separated shortly after launch, interesting differences in the particle intensities at STEREO A and B and near-Earth spacecraft were observed during the final large SEP events of Solar Cycle 23 in December 2006 (von Rosenvinge *et al.*, 2009). Separating from Earth by $\sim 22^{\circ}$ year^{-1}, STEREO A and B were 180° apart above the west and east limbs of the Sun, respectively, as viewed from Earth on 6 February 2011, allowing observations of the complete solar surface to be made for the first time.

In this paper, we focus on observations of 14 – 41 MeV protons and 0.3 – 4 MeV electrons made by the *High Energy Telescopes* (HETs) on the STEREO spacecraft (von Rosenvinge *et al.*, 2008) during the first $\sim$seven years of the STEREO mission. By combining these observations with similar observations from the EPHIN (Müller-Mellin *et al.*, 1995) and ERNE (Torsti *et al.*, 1995) instruments on the SOHO spacecraft in orbit around the L1 point upstream of Earth, we have compiled a catalog of 209 individual >25 MeV proton events that were observed at one or multiple spacecraft from the start of the STEREO mission up to the end of 2013, when the STEREO spacecraft were separated by $\sim 60^{\circ}$ on the far side of the Sun relative to Earth. We then summarize the general features of a subset of events observed at all three locations, including how the particle onset delay and peak intensity depend on the location of the associated solar event relative to the observing spacecraft. The results provide constraints for models of particle transport processes at/near the Sun or in the solar wind and suggest a formula for the SEP intensity as a function of the speed of the associated coronal mass ejection and location of the solar event relative to the observer, which is tested using a sample of more than 500 events in Cycles 23 and 24.

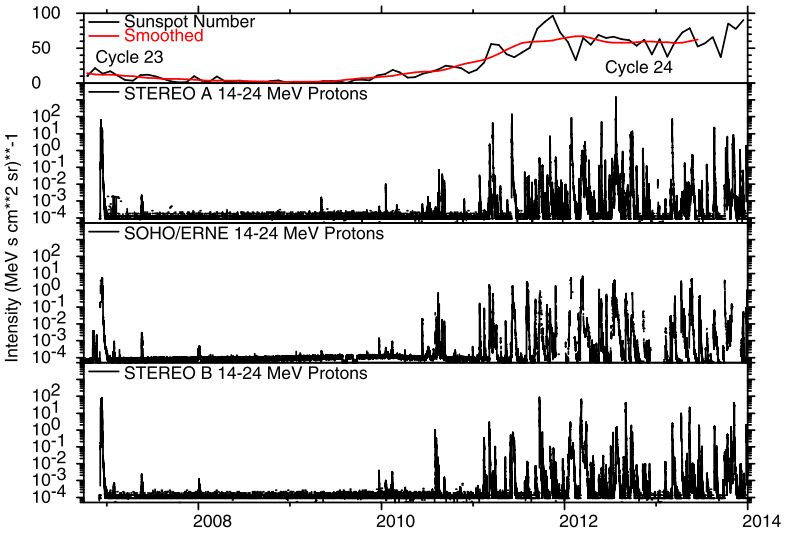

Figure 1 Intensities of 14 – 24 MeV protons (1 hr averages) observed by the HET instruments on STEREO A (*Ahead*) and B (*Behind*) (second and bottom panels, respectively) and the ERNE instrument on SOHO (third panel), from October 2006 to December 2013. The top panel shows the monthly and smoothed international sunspot numbers.

2. Observations

We used energetic particle observations made by the HET instruments on STEREO A and B and the ERNE and EPHIN instruments on SOHO from STEREO launch in October 2006 until December 2013. For protons, we focused on two energy ranges, 14 – 24 and 24 – 41 MeV, defined by a combination of HET energy channels to enhance the counting statistics. HET data are available from http://www.srl.caltech.edu/STEREO/. Energy channels 36 – 42 and 44 – 50 of the ERNE *High Energy Detector* closely match these energy ranges (13.8 – 24.2 and 24.1 – 40.5 MeV, respectively); the ERNE data were obtained from the Space Research Laboratory, University of Turku (http://www.srl.utu.fi/erne_data/). EPHIN has proton channels at 7.8 – 25 MeV and 25 – 53 MeV; the EPHIN data were obtained from the University of Kiel (http://www.ieap.uni-kiel.de/et/ag-heber/costep/). For electrons, we used intensities at 0.7 – 4 MeV from the STEREO A/B HETs, and at 0.67 – 3 MeV from EPHIN.

Figure 1 gives an overview of 14 – 24 MeV proton intensities observed by the STEREO A and B HETs (second and bottom panels) and ERNE (third panel), from October 2006 to December 2013. The top panel shows the monthly average and smoothed sunspot number, indicating that this interval extended from the late decay phase of Solar Cycle 23 to the first $\sim$ five years of Cycle 24 (smoothed sunspot minimum was in December 2008). Following the intense particle events in December 2006 (*e.g.*, von Rosenvinge *et al.*, 2009), there were few SEP events extending into this energy range during the extended sunspot minimum between these cycles. The SEP occurrence rate finally increased in December 2009, around one year into Cycle 24. By this time, STEREO A was 64° ahead of Earth, while STEREO B was lagging Earth by 67°. Note that while the SEP events in December 2009 – February 2010 were relatively weak, those on 22 December 2009 and 17 January 2010 were observed at all three spacecraft. This increase in activity was temporary, however. Few SEP events were observed during March to August 2010, when activity increased once again, but also

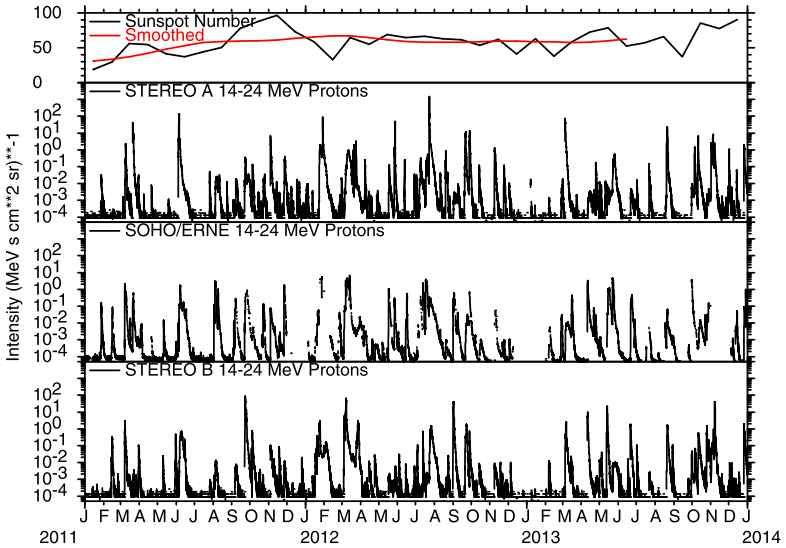

Figure 2 As in Figure 1 for January 2011 to December 2013.

temporarily. SEP events were observed more persistently from around February 2011. Thus, the first ∼ two years of Cycle 24 were characterized by brief episodes of > 14 MeV proton events during an otherwise quiet period. Interestingly, the intervals between these episodes of activity are both ∼ 6 – 7 months. Quasi-periodicities of ∼ 150 days have been reported for energetic solar phenomena in some other cycles, for example by Rieger *et al.* (1984), Lean (1990) (who identified periods of ∼ 130 – 185 days in a survey of multiple solar cycles), Cane, Richardson, and von Rosenvinge (1998), Dalla *et al.* (2001), Richardson and Cane (2005), Richardson and Cane (2010), and references therein, so the rise of Cycle 24 may also show evidence of a similar phenomenon.

Figure 2 shows an expanded view of observations from January 2011 (when STEREO A was 86° ahead of Earth and STEREO B was behind by 91°) to December 2013 in the format of Figure 1. By the end of December 2013, STEREO A was 150° ahead of Earth, STEREO B was behind by 152°, and the STEREO spacecraft were separated by 58°. Despite the large separation between the spacecraft, overall, the particle intensity–time profiles are remarkably similar, with intervals of higher intensity that include contributions from the same solar events, as we discuss below, interspersed with quieter intervals that are also evident at all locations.

The intercalibration between the various instruments we used can be checked over a wide dynamic range during the events in December 2006, when the STEREO spacecraft were still close to Earth. Figure 3 compares intensities measured during December 2006 by various instruments. Figure 3(a) shows one-hour averages of the HET A 13.6 – 23.8 MeV proton intensity plotted against the HET B intensity at the same energy. As might be expected, the HET A and HET B intensities are highly correlated (cc = 0.991), with similar intensities at both spacecraft ($I\,(\mathrm{B}) = 1.006 I\,(\mathrm{A})^{0.992}$; the red line in each panel in Figure 3 indicates equality between the intensities). Note that STEREO B was inverted at this time so that HET B was viewing perpendicular to the nominal Parker spiral direction, whereas the STEREO A HET was viewing along the spiral direction. Differences in the intensities measured by the HETs might be expected at times of significantly anisotropic particle distributions, such

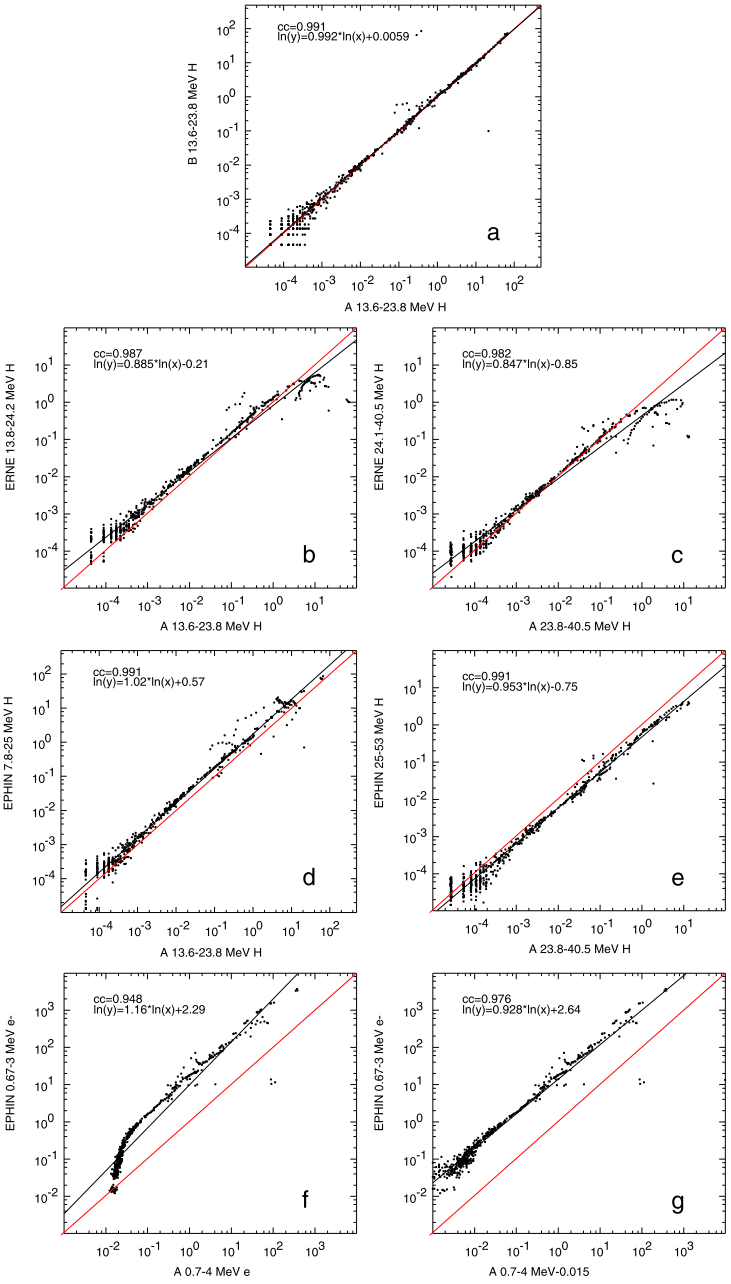

Figure 3 Comparison of the STEREO HETs, SOHO/ERNE E, and SOHO/EPHIN proton and electron intensities (in $(\mathrm{MeV\,s\,cm^2\,sr})^{-1}$) using observations during December 2006. (a) HET B *vs.* HET A for 13.6 – 23.8 MeV protons; (b) ERNE 13.8 – 24.2 MeV protons *vs.* HET A 13.6 – 23.8 MeV protons; (c) ERNE 24.1 – 40.5 MeV protons *vs.* HET A 23.8 – 40.5 MeV protons; (d) EPHIN 7.8 – 25 MeV protons *vs.* HET A 13.6 – 23.8 MeV protons; (e) EPHIN 25 – 53 MeV protons *vs.* HET A 23.8 – 40.5 MeV protons; (f) EPHIN 0.67 – 3.0 MeV electrons *vs.* HET A 0.7 – 4.0 MeV electrons, and (g) with a HET background of 0.015 $(\mathrm{MeV\,s\,cm^2\,sr})^{-1}$ subtracted. Black lines are least-squares fits to the data, while red lines indicate equal values.

as those discussed by von Rosenvinge *et al.* (2009), but evidently the observed intensities were generally comparable despite the different spacecraft configurations.

Figure 3(b) shows the 13.8 – 24.2 MeV proton intensity from the SOHO/ERNE HED plotted against the same HET A intensity. The intensities are correlated, though with the ERNE intensity ∼ 1.5 times the HET A intensity, until ∼ 1 (MeV s cm^2 sr)$^{-1}$ when ERNE saturates. Figure 3(c) shows the 24.1 – 40.5 MeV proton intensity from ERNE plotted *vs.* the 23.8 – 40.5 MeV proton intensity from HET A, again showing close agreement until ERNE saturates above ∼ 0.1 (MeV s cm^2 sr)$^{-1}$. Figure 3(d) shows the 7.8 – 25 MeV proton intensity from EPHIN *vs.* the HET A 13.6 – 23.8 MeV proton intensity. The EPHIN intensity is correlated with, but ∼ 1.7 times higher than the HET A intensity at a slightly higher energy. Hence, the EPHIN data, with this conversion factor, may be used to provide an estimate of the intensity in the HET A energy range when ERNE is saturated or data are not available. Similarly, Figure 3(e) shows that the 25 – 53 MeV EPHIN proton intensity is around a half of the HET A 23.8 – 40.5 MeV intensity. Finally, Figures 3(f) and (g) compare electron intensities at 0.7 – 4 MeV from HET A and 0.67 – 3 MeV from EPHIN, (f) showing the observed intensities, and (g) with a background of 0.015 (MeV s cm^2 sr)$^{-1}$ removed from HET A. With this correction, the HET A and EPHIN electron intensities are well correlated, but the EPHIN intensity is a factor of ∼ 14 higher than the HET A intensity. (The reason for this relatively large conversion factor, which appears to be associated with the HETs, since the EPHIN calibration is consistent with other instruments, is under investigation at the time of writing.) A similar analysis for HET B suggests a similar conversion factor and a background of 0.02 (MeV s cm^2 sr)$^{-1}$. The few points lying off the main distribution in (f) and (g) are associated with high electron intensities observed when STEREO A crossed the geomagnetic tail.

SOHO makes a 180° roll approximately every three months (because of an immovable high gain antenna) causing the fields of view of EPHIN and ERNE to change direction. We have not attempted to make any correction to the EPHIN and ERNE intensities when this occurs. One reason is the STEREO observations in Figure 3(a), made when STEREO B was inverted, suggest that the correction might be small. Furthermore, when the STEREO and SOHO spacecraft are well separated, they measure different particle populations with different anisotropies. An accurate correction would require information on the particle pitch angle distribution and IMF at each spacecraft. Thus we used the observed particle intensities at each spacecraft without any correction (other than the calibrations suggested by Figure 3) with the expectation that these are accurate to within a factor of ∼ 2.

2.1. Event Catalog

In past studies (*e.g.*, Cane, Reames, and von Rosenvinge, 1988; Cane, Richardson, and von Rosenvinge, 2010a), we have documented the properties of particle events that include ∼ 25 MeV protons. In particular, Cane, Richardson, and von Rosenvinge (2010a) discussed 280 such events that occurred in 1997 – 2006 (see also Vainio *et al.*, 2013). To compile a similar catalog of SEP events at the STEREO spacecraft and/or at Earth that include protons of such energies, we have examined proton and electron intensity–time data from each spacecraft, as described above, with integration periods of 1 minute to 1 hour. At such energies, the SEP intensity is generally not dominated by locally accelerated ions associated with interplanetary shocks, and peak intensities typically occur early in the event, providing information on particle acceleration close to the Sun.

To identify the associated solar event and its location, we examined movies from the SOHO EIT instrument (Delaboudinière *et al.*, 1995), the EUVI instruments on the STEREO

spacecraft (Wülser *et al.*, 2004), and the AIA on the *Solar Dynamics Observatory* (Lemen *et al.*, 2012); observations of coronal mass ejections from the LASCO coronagraphs on SOHO (Brueckner *et al.*, 1995) and the SECCHI COR1 and COR2 coronagraphs on the STEREO spacecraft (Howard *et al.*, 2008); Hα and GOES soft X-ray flare reports (limited to front-side or near-limb events), and observations of solar radio emissions made by the WAVES instrument on WIND (http://lep694.gsfc.nasa.gov/waves/) and the SWAVES instruments on the STEREO spacecraft (http://swaves.gsfc.nasa.gov/). Observations by WAVES and SWAVES of the type III radio emissions that accompany nearly every SEP event (*e.g.*, Cane, Erickson, and Prestage, 2002; Cane and Erickson, 2003; Cane, Richardson, and von Rosenvinge, 2010a; see also below) are of particular value since the intensity and degree of occultation at higher frequencies by the limb of the Sun observed at the three locations can help to confirm the location of the SEP source at the Sun. We used the onset times of the energetic particles at the three spacecraft, in particular that showing the most prompt increase, to infer an approximate time for the event at the Sun. Particle event onset times are estimated by inspection of intensity–time profiles around event onset using suitable intensity/timescales and data-averaging intervals to estimate when the intensity rises above the range of intensity fluctuations in the pre-event background. We then examined the solar and radio observations for evidence of, for example, a flare, eruption in EIT, EUV or EUVI, a coronal mass ejection (CME), and type III and/or type II radio emissions (type II radio emissions were obtained from the WIND WAVES/STEREO SWAVES list at http://lep694.gsfc.nasa.gov/waves/data_products.html) that is consistent with the SEP event onset. For every SEP event including 25 MeV protons identified so far, it is possible to associate an unambiguous solar event. In particular, the STEREO spacecraft can, for the first time, provide imaging evidence that an event originated on the far side of the Sun from Earth. We also examined SEP data over a range of energies and solar-wind observations at the STEREO spacecraft and at Earth to identify and remove any intensity increases that are likely to be associated with the passage of shocks, or are spatial modulations that, for example, have no velocity dispersion or are related to solar-wind structures. Such features are also not usually associated with appropriately timed solar activity.

For most of the events since August 2010, we compared the inferred solar source longitudes with the propagation direction of the related CMEs obtained by triangulation of the STEREO and LASCO coronagraph observations included in the "Space Weather Database Of Notifications, Knowledge, Information (DONKI)" (http://kauai.ccmc.gsfc.nasa.gov/DONKI/) developed at the Community Coordinated Modeling Center. As expected, the CME propagation longitudes are usually consistent with the source longitudes (in 82 % of cases, the directions differed by $\leq 20°$) suggesting that the source identifications are very likely correct. For 5 % of the events, the directions differed by over 60°. These cases were then re-checked, including consideration of the particle, radio and solar data, and the source location was either reconciled with the CME direction, or the original location was retained if the supporting evidence was more compelling.

The 209 unique >25 MeV proton events identified up to December 2013 are listed in Table 1 (a subset of these events were also considered by Lario *et al.*, 2013). The first two columns give the times (date and hour of day) of the associated solar event and the particle event onset at the spacecraft with the most prompt particle arrival. In most cases, these times differ by only an hour or two, but in some cases, the delay is longer, or the solar event occurs on the day preceding the SEP onset. The next three pairs of columns show for STEREO B, Earth (*i.e.*, SOHO), and STEREO A, the heliolongitude of the solar event relative to the observing spacecraft (a negative value indicates that the event is east of the spacecraft), and the peak intensity for ~ 25 MeV protons in $(\mathrm{MeV\,s\,cm^2\,sr})^{-1}$. The intensity is generally

Table 1 > 25 MeV proton events at 1 AU during the STEREO mission.

Solar event (UT)	SEP event (UT)	Flare–B (°)	I(B)	Flare–Earth (°)	I(Earth)	Flare–A (°)	I(A)	GOES X-Ray	Type III	Type II	CME dA (°)	CME V km s^{-1}
5 December 2006, 10	5 December, 12	−68	0.04	−68	0.04	−68	0.04	X9.0	1	2	DG	DG
6 December 2006, 18	6 December, 19	−64	BG	−64	BG	−64	BG	X6.5	1	2	360	DG
13 December 2006, 02	13 December, 02	23	10	23	10	23	10	X3.4	1	2	360	1774
14 December 2006, 21	14 December, 22	46	0.5	46	0.5	46	0.5	X1.5	1	2	360	1042
19 May 2007, 12	19 May, 14	08	0.0004	05	0.0009	−01	0.0003	B9.5	1	1	106	958
23 May 2007, 07	23 May, 07	63	0.0003	60	0.0003	54	0.0003	B5.3	1	0	90	679
31 December 2007, 00	31 December, 02	−85	...	−108	0.0001	−129	...	C8.3	1	1	164	995
5 May 2009, 08	5 May, 10	−90	...	−137	...	175	0.0006	...	1	1	66 B	595 B
22 December 2009, 04	22 December, 05	113	0.0008	46	0.0005	−18	0.0002	C7.2	1	0	47	318
17 January 2010, 03	17 January, 04	−50	0.0003	−120	0.0003	176	0.003	...	1	1	126	350
6 February 2010, 07	6 February, 08	53	0.0003	−18	...	−83	...	C4.0	1	0	56	240
7 February 2010, 02	7 February, 03	61	0.0003	−10	...	−75	...	M1.3	1	0	360	421
12 February 2010, 11	12 February, 12	60	0.001	−11	0.0003	−76	...	M8.3	1	0	360	509
12 June 2010, 00	12 June, 01	113	0.0001	43	0.007	−31	0.0002	M2.0	1	1	119	486
1 August 2010, 07	1 August, 12	35	0.02	−36	0.0005	−114	...	C3.2	0	2	360	850
7 August 2010, 17	7 August, 19	38	0.08	−34	0.005	−113	...	M1.0	1	2	360	871
14 August 2010, 09	14 August, 10	126	0.004	54	0.16	−26	0.001	C4.4	1	0	360	1205
18 August 2010, 05	18 August, 06	172	0.001	100	0.03	20	0.008	C4.5	1	2	184	1471
31 August 2010, 02	31 August, 03	−141	...	145	...	64	0.0002	...	1	0	33	319
31 August 2010, 21	31 August, 22	−141	0.0001	145	0.005	64	0.008	...	1	1	360	1304
4 September 2010, 14	4 September, 20	144	...	70	0.0001	−11	...	B2.5	1	0	130	567
8 September 2010, 23	8 September, 24	167	0.0003	92	0.003	10	0.003	C3.3	1	1	147	818
31 December 2010, 04	31 December, 05	159	...	69	0.0001	−17	...	C1.3	1	0	45	363

Table 1 (*Continued.*)

Solar event (UT)	SEP event (UT)	Flare–B (°)	I(B)	Flare–Earth (°)	I(Earth)	Flare–A (°)	I(A)	GOES X-Ray	Type III	Type II	CME dA (°)	CME V km s^{-1}
27 January 2011, 08	27 January, 10	169	...	76	0.0001	−10	...	B6.6	1	0	52	316
27 January 2011, 11	27 January, 14	178	...	85	0.0001	−1	...	C1.2	1	1	43	349
28 January 2011, 00	28 January, 02	−177	...	90	0.05	04	0.02	M1.3	1	1	119	606
31 January 2011, 16	31 January, 20	−136	...	131	...	45	0.0002	...	1	1	150	713
13 February 2011, 17	13 February, 18	90	0.0004	−04	0.00015	−91	...	M6.6	1	1	276	373
14 February 2011, 17	14 February, 18	112	0.001	18	0.0003	−69	...	M2.2	1	0	360	326
15 February 2011, 01	15 February, 02	112	0.08	18	0.021	−69	...	X2.2	1	2	360	669
24 February 2011, 07	24 February, 08	15	0.0006	−102	...	−171	...	M3.5	1	0	158	1186
4 March 2011, 14	4 March, 15	−85	...	180	...	90	0.0003	...	1	0	60 B	297 B
7 March 2011, 13	7 March, 15	74	0.04	−21	0.0004	−109	...	M1.9	1	1	261	698
7 March 2011, 19	7 March, 21	148	0.4	53	0.5	−35	0.006	M3.7	1	2	360	2125
16 March 2011, 17	16 March, 22	−167	...	72	0.004	−16	0.0002	C3.7	1	0	184	682
21 March 2011, 02	21 March, 03	−127	0.0008	138	0.11	50	12	...	1	2	360	1341
29 March 2011, 20	30 March, 04	−25	0.01	−120	...	151	0.003	...	0	0	> 195	1264
3 April 2011, 05	3 April, 06	170	...	75	0.0008	−14	...	C1.2	1	0	DG	DG
4 April 2011, 03	4 April, 12	165	...	70	0.001	−19	...	B8.6	1	0	DG	DG
21 April 2011, 00	21 April, 02	−105	...	160	0.0007	70	0.001	...	1	0	111	475
9 May 2011, 20	10 May, 00	0	0.002	−94	...	174	...	C5.4	1	2	292	1318
11 May 2011, 02	11 May, 04	147	...	53	0.004	−39	...	B8.1	1	0	225	745
19 May 2011, 03	19 May, 06	154	...	60	...	−33	0.0001	B3.0	1	0	132	626
29 May 2011, 20	29 May, 22	25	0.01	−68	...	−162	...	C8.7	1	2	186	1407
2 June 2011, 07	2 June, 09	68	0.0006	−25	...	−119	...	C3.7	1	1	360	976
4 June 2011, 06	4 June, 07	−112	...	155	0.002	60	0.1	...	1	2	360	1407
4 June 2011, 22	4 June, 22	−100	0.08	165	0.04	70	13	...	1	2	360	2425

Table 1 (*Continued.*)

Solar event (UT)	SEP event (UT)	Flare–B (°)	I(B)	Flare–Earth (°)	I(Earth)	Flare–A (°)	I(A)	GOES X-Ray	Type III	Type II	CME dA (°)	CME V km s^{-1}
7 June 2011, 06	7 June, 07	147	BG	54	0.7	−41	BG	M2.5	1	2	360	1255
29 June 2011, 00	29 June, 00	169	...	77	0.0001	−20	...	B7.3	1	0	122	481
11 July 2011, 10	11 July, 12	86	...	−06	0.0001	−104	...	C2.6	1	0	53	266
26 July 2011, 08	26 July, 10	−82	0.0004	−175	...	85	0.01	...	1	1	360	382
2 August 2011, 05	2 August, 07	108	0.0008	15	0.04	−85	...	M1.4	1	1	268	712
3 August 2011, 13	3 August, 14	123	...	30	0.007	−70	...	M6.0	1	0	360	610
4 August 2011, 03	4 August, 05	129	0.004	36	1.1	−64	0.005	M9.3	1	2	360	1315
8 August 2011, 18	8 August, 19	154	...	61	0.05	−39	...	M3.5	1	2	237	1343
9 August 2011, 07	9 August, 08	162	...	69	0.5	−31	0.002	X6.9	1	1	360	1610
23 August 2011, 22	24 August, 06	−85	...	−179	...	70	0.002	...	0	0	360	312
3 September 2011, 02	3 September, 03	−75	...	170	0.0002	68	0.0003	...	1	0	105	325
4 September 2011, 04	4 September, 05	162	...	67	0.002	−35	...	C9.0	0	0	53	262
4 September 2011, 23	5 September, 02	−165	...	100	0.0006	−03	0.0002	C7.9	1	0	146	622
6 September 2011, 01	6 September, 02	102	0.003	7	0.03	−95	...	M5.3	1	2	360	782
6 September 2011, 22	6 September, 23	113	0.005	18	0.1	−84	0.0002	X2.1	1	2	360	575
7 September 2011, 18	7 September, 20	−50	BG	−145	BG	112	0.004	...	1	1	188	924
8 September 2011, 22	9 September, 00	−122	BG	143	BG	40	0.003	...	1	1	281	983
13 September 2011, 12	13 September, 12	−161	...	103	0.0003	0	...	...	1	0	199	746
21 September 2011, 22	21 September, 23	−155	...	109	0.002	05	0.0004	...	1	0	255	1007
22 September 2011, 10	22 September, 10	18	10.0	−78	0.08	−179	0.04	X1.4	1	2	360	1905
24 September 2011, 09	24 September, 11	37	0.5	−60	BG	−164	BG	X1.9	1	2	145	1936
4 October 2011, 12	4 October, 15	−50	0.2	−148	0.001	108	0.02	...	1	0	360	1101
14 October 2011, 11	14 October, 15	−40	0.0002	−140	...	115	0.0005	...	1	0	241	814
20 October 2011, 03	20 October, 04	−155	...	105	0.0008	0	0.0002	M1.6	1	0	193	893

Table 1 (*Continued.*)

Solar event (UT)	SEP event (UT)	Flare–B (°)	I(B)	Flare–Earth (°)	I(Earth)	Flare–A (°)	I(A)	GOES X-Ray	Type III	Type II	CME dA (°)	CME V km s^{-1}
22 October 2011, 10	22 October, 12	177	0.0003	77	0.006	−28	0.0008	M1.3	0	2	360	1105
3 November 2011, 22	3 November, 23	−50	0.06	−152	0.04	103	2.0	...	1	2	360	991
9 November 2011, 13	9 November, 14	83	0.002	−20	0.002	−126	...	M1.1	1	2	360	907
12 November 2011, 18	12 November, 18	0	0.0002	−103	...	151	0.0003	...	1	0	192	654
13 November 2011, 18	13 November, 22	−70	0.0003	−174	...	80	0.001	...	1	0	360	596
17 November 2011, 22	17 November, 23	−20	0.01	−125	0.0005	129	0.001	...	1	0	360	1041
23 November 2011, 15	23 November, 15	−60	...	−165	...	90	0.0003	...	1	0	95?	315?
26 November 2011, 06	26 November, 08	154	0.002	48	0.33	−58	0.01	C1.2	1	2	360	933
3 December 2011, 07	3 December, 08	−117	...	136	DG	30	0.0003	...	1	0	155	454
11 December 2011, 13	11 December, 14	−76	...	176	...	70	0.0003	...	1	0	32 A	312 A
17 December 2011, 10	17 December, 16	−115	...	136	0.0003	30	0.002	...	1	0	247	987
24 December 2011, 11	24 December, 14	−165	...	85	0.0003	−22	...	C4.9	1	2	102	447
25 December 2011, 18	25 December, 19	136	0.006	26	0.05	−81	...	M4.0	1	1	125	366
27 December 2011, 04	27 December, 05	78	0.0006	−32	BG	−139	...	C8.9	1	0	84 B	735 B
29 December 2011, 16	29 December, 18	−142	...	107	0.001	0	...	...	1	0	171	736
2 January 2012, 14	2 January, 16	−152	...	97	0.015	−10	0.001	C2.4	1	1	360	1138
12 January 2012, 07	12 January, 10	−05	0.0003	−118	...	135	0.0006	C2.5	0	0	360	814
16 January 2012, 02	16 January, 08	45	0.0005	−68	0.0003	−175	...	C6.5	0	0	360	1060
19 January 2012, 13	19 January, 15	84	0.03	−30	0.0006	−137	...	M3.2	1	2	360	1120
23 January 2012, 04	23 January, 04	135	0.6	21	20	−87	0.1	M8.7	1	2	360	2175
27 January 2012, 17	27 January, 19	−175	BG	71	10	−37	0.3	X1.7	1	2	360	2508
24 February 2012, 04	24 February, 10	79	...	−38	0.0005	−147	...	...	0	2	189	800
29 February 2012, 09	29 February, 10	−118	...	125	0.0005	16	0.005	...	1	0	360	446
3 March 2012, 18	4 March, 00	45	0.0002	−73	...	178	...	C1.9	1	0	49	1078

Table 1 (*Continued.*)

Solar event (UT)	SEP event (UT)	Flare–B (°)	I(B)	Flare–Earth (°)	I(Earth)	Flare–A (°)	I(A)	GOES X-Ray	Type III	Type II	CME dA (°)	CME V km s^{-1}
4 March 2012, 10	4 March, 12	48	0.4	−61	0.02	−170	...	M2.0	1	2	360	1306
5 March 2012, 02	5 March, 04	57	0.3	−52	BG	−161	0.001	X1.1	1	2	360	1531
7 March 2012, 00	7 March, 01	91	10.0	−27	10	−137	0.09	X5.4	1	2	360	2684
13 March 2012, 17	13 March, 18	179	BG	61	10	−48	BG	M7.9	1	2	360	1884
21 March 2012, 07	21 March, 07	−81	BG	160	BG	50	0.8	...	1	1	360	1178
24 March 2012, 00	24 March, 00	−50	0.03	−169	0.001	80	1.3	...	1	2	360	1152
26 March 2012, 22	27 March, 00	−5	0.6	−124	BG	125	BG	...	1	1	360	1390
5 April 2012, 20	6 April, 00	148	...	29	0.002	−82	...	C1.5	1	0	360	828
7 April 2012, 16	7 April, 17	−80	...	161	0.0005	50	0.02	...	1	2	360	765
9 April 2012, 12	9 April, 12	−171	...	73	0.0006	−38	...	C3.9	1	1	360	921
15 April 2012, 02	15 April, 03	29	0.002	−90	...	158	0.001	C1.7	1	1	173	1220
18 April 2012, 02	18 April, 03	−39	...	−150	...	90	0.0006	...	1	0	> 271	352
18 April 2012, 14	18 April, 15	−35	...	−154	0.0001	94	0.0004	...	1	2	184	840
24 April 2012, 07	24 April, 09	30	0.015	−88	0.0002	159	...	C3.7	1	0	190	443
27 April 2012, 15	27 April, 18	−108	...	133	...	20	0.0003	...	1	1	360	681
1 May 2012, 16	1 May, 18	−59	...	−177	...	70	0.0002	...	1	0	200	788
7 May 2012, 00	7 May, 03	142	...	24	0.0002	−90	...	C1.3	1	0	124 A	625 A
14 May 2012, 09	14 May, 10	158	...	40	0.0003	−75	...	C2.5	1	0	48	551
17 May 2012, 01	17 May, 02	−166	0.001	76	0.6	−39	0.002	M5.1	1	2	360	1582
26 May 2012, 20	26 May, 21	−127	0.001	116	0.03	00	0.2	...	1	2	360	1966
1 June 2012, 22	1 June, 22	−162	...	81	0.0006	−35	...	C3.3	1	0	175	630
3 June 2012, 17	3 June, 19	79	0.01	−38	...	−154	...	M3.3	1	0	180	605
8 June 2012, 07	8 June, 07	157	...	40	0.0001	−77	...	C4.8	0	0	9	329
12 June 2012, 05	12 June, 06	−109	...	135	0.0001	18	0.001	...	1	0	195	864

Table 1 (*Continued.*)

Solar event (UT)	SEP event (UT)	Flare–B (°)	I(B)	Flare–Earth (°)	I(Earth)	Flare–A (°)	I(A)	GOES X-Ray	Type III	Type II	CME dA (°)	CME V km s^{-1}
14 June 2012, 12	14 June, 15	111	0.001	−06	0.002	−123	...	M1.9	1	0	360	987
28 June 2012, 07	28 June, 08	−65	...	179	...	60	0.002	...	1	0	360	728
28 June 2012, 16	28 June, 16	71	0.001	−45	...	−164	...	M2.4	1	0	104	714
2 July 2012, 08	2 July, 09	−10	0.001	−126	0.0001	115	0.01	...	1	2	360	1704
4 July 2012, 16	4 July, 18	150	...	34	0.003	−85	...	M1.8	1	1	360	662
5 July 2012, 21	5 July, 22	161	...	46	BG	−73	0.0002	M1.6	1	2	94	980
6 July 2012, 23	7 July, 01	165	...	50	0.3	−69	0.004	X1.1	1	2	360	1828
8 July 2012, 16	8 July, 16	−171	...	74	0.1	−46	0.1	M6.9	1	2	157	1495
12 July 2012, 15	12 July, 17	109	0.2	−06	0.8	−126	BG	X1.4	1	2	360	885
13 July 2012, 19	13 July, 20	−115	BG	130	BG	10	0.004	...	1	0	115	386
17 July 2012, 12	17 July, 15	180	...	65	0.8	−55	0.001	M1.7	1	2	176	958
18 July 2012, 06	18 July, 06	−75	0.001	170	BG	50	0.1	...	1	1	360	873
19 July 2012, 04	19 July, 08	−145	...	100	0.8	−20	BG	M7.7	1	2	360	1631
23 July 2012, 02	23 July, 03	−105	0.5	140	0.15	20	50	...	1	2	360	2003
10 August 2012, 09	10 August, 13	−97	...	147	0.0012	25	0.008	...	1	0	251	464
19 August 2012, 04	19 August, 05	−71	...	173	0.0002	50	0.08	...	1	0	224	577
19 August 2012, 18	19 August, 18	−71	0.001	173	0.0002	50	0.4	...	1	0	360	612
21 August 2012, 20	21 August, 21	−56	0.0008	−172	...	65	BG	...	1	2	360	521
31 August 2012, 19	31 August, 20	74	20	−42	0.037	−165	0.0008	C8.4	1	2	360	1442
8 September 2012, 10	8 September, 11	−99	...	145	0.014	20	0.002	...	1	1	360	734
19 September 2012, 11	19 September, 12	−51	...	−168	...	67	0.002	...	1	1	360	616
19 September 2012, 22	19 September, 22	−46	...	−163	...	72	0.04	...	1	0	141	496
20 September 2012, 15	20 September, 15	−40	0.2	−158	0.003	77	5	...	1	2	360	1202
27 September 2012, 10	27 September, 10	−84	...	158	BG	33	0.15	...	1	2	360	1319

Table 1 (*Continued.*)

Solar event (UT)	SEP event (UT)	Flare–B (°)	I(B)	Flare–Earth (°)	I(Earth)	Flare–A (°)	I(A)	GOES X-Ray	Type III	Type II	CME dA (°)	CME V km s^{-1}
27 September 2012, 23	28 September, 00	152	0.3	34	0.2	−91	BG	C3.7	1	2	360	755
7 October 2012, 06	7 October, 12	124	...	5	0.0002	−121	...	B4.5	1	0	149	663
14 October 2012, 00	14 October, 01	−18	0.008	−138	0.0002	96	0.06	...	1	1	360	987
27 September 2012, 23	28 September, 00	152	0.3	34	0.2	−91	BG	C3.7	1	2	360	755
7 October 2012, 06	7 October, 12	124	...	5	0.0002	−121	...	B4.5	1	0	149	663
14 October 2012, 00	14 October, 01	−18	0.008	−138	0.0002	96	0.06	...	1	1	360	987
8 November 2012, 02	8 November, 03	35	0.006	−88	...	145	0.0003	M1.7	1	0	360	855
8 November 2012, 11	8 November, 11	−68	BG	168	0.015	41	0.4	...	1	0	360	972
16 November 2012, 06	17 November, <19	10	0.005	−114	...	118	...	C1.4	1	0	360	775
20 November 2012, 12	20 November, 13	−135	...	10	0.0001	−118	...	M1.7	1	0	360	619
21 November 2012, 15	21 November, 17	124	0.001	−1	0.0003	−128	...	M3.5	0	0	360	529
23 November 2012, 23	23 November, 23	−102	...	132	0.0003	5	0.03	...	1	2	360	1186
24 November 2012, 13	24 November, 14	154	...	28	0.0003	−100	...	C3.3	1	0	84	237
2 December 2012, 15	2 December, 16	−56	...	177	0.0005	50	0.005	...	1	0	360	678
5 December 2012, 00	5 December, 03	52	0.003	−75	...	157	0.0002	C1.7	1	1	231	963
14 December 2012, 01	14 December, 03	169	...	40	0.01	−88	...	...	1	0	149	763
6 January 2013, 22	6 January, 23	−40	...	−173	...	58	0.008	...	1	0	211	667
16 January 2013, 18	16 January, 20	−149	...	77	0.005	−52	...	C2.2	1	0	250	648
6 February 2013, 00	6 February, 03	118	0.002	−19	0.0001	−149	0.0004	C8.7	1	0	271	1867
26 February 2013, 09	26 February, 13	−89	...	131	0.01	0	0.002	...	1	1	360	987
5 March 2013, 03	5 March, 03	−1	0.4	−141	0.006	88	30	...	1	1	360	1316
15 March 2013, 05	15 March, 07	129	0.006	−12	0.004	−144	...	M1.1	1	2	360	1063
11 April 2013, 06	11 April, 07	130	5	−12	2	−146	0.001	M6.5	1	2	360	861
21 April 2013, 06	21 April, 08	−94	...	124	0.02	−10	0.001	...	1	0	360	919

Table 1 (*Continued.*)

Solar event (UT)	SEP event (UT)	Flare–B (°)	I(B)	Flare–Earth (°)	I(Earth)	Flare–A (°)	I(A)	GOES X-Ray	Type III	Type II	CME dA (°)	CME V km s^{-1}
24 April 2013, 21	24 April, 22	−44	0.001	175	0.01	40	0.1	...	1	0	360	594
28 April 2013, 20	28 April, 22	179	...	37	0.0004	−97	...	C4.4	1	0	91	497
24 April 2013, 21	24 April, 22	−44	0.001	175	0.01	40	0.1	...	1	0	360	594
28 April 2013, 20	28 April, 22	179	...	37	0.0004	−97	...	C4.4	1	0	91	497
1 May 2013, 02	1 May, 04	37	0.009	−105	...	120	0.007	...	1	1	360	762
2 May 2013, 04	2 May, 06	168	BG	26	0.0005	−109	BG	M1.1	1	0	99	671
3 May 2013, 17	3 May, 20	61	0.003	−81	...	144	0.002	M5.7	0	0	274	858
10 May 2013, 18	10 May, 20	−78	...	140	0.0002	5	0.006	...	1	0	120	617
13 May 2013, 01	13 May, 02	39	0.2	−103	BG	121	...	X1.7	1	1	360	1270
13 May 2013, 15	13 May, 16	47	1.0	−95	0.01	129	0.004	X2.8	1	2	360	1850
15 May 2013, 01	15 May, 06	78	BG	−64	0.3	160	BG	X1.2	1	2	360	1366
22 May 2013, 12	22 May, 13	−149	0.003	70	20	−67	0.06	M5.0	1	2	360	1466
17 June 2013, 02	17 June, 03	81	0.002	−59	...	161	...	C1.2	0	...	...	...
21 June 2013, 02	21 June, 03	67	0.6	−73	0.06	147	0.001	M2.9	1	...	160*	1249*
1 July 2013, 20	1 July, 20	50	0.015	−90	...	130	0.004	...	1	...	188*	542*
3 July 2013, 07	3 July, 07	58	0.002	−82	...	137	...	M1.5	1	...	102*	580*
22 July 2013, 06	22 July, 06	−50	0.001	172	0.001	29	0.04	...	1	...	360 M	1032 M
17 August 2013, 19	17 August, 19	168	...	30	0.002	−174	...	M3.3	-1	...	156*	726*
19 August 2013, 23	20 August, 00	−48	0.4	174	0.01	30	3	...	1	...	144*	637*
30 August 2013, 02	30 August, 02	95	0.03	−43	0.0003	172	...	C8.2	1	...	360 M *	1071 M*
24 September 2013, 19	25 September, 00	79	0.0002	−60	0.0001	153	...	...	1	...	126*	661*
29 September 2013, 21	29 September, 22	164	0.02	25	0.5	−122	0.003	C1.2	1	...	360 M	897 M
5 October 2013, 08	5 October, 08	16	0.02	−123	...	90	0.5	...	1	...	324*	640*
11 October 2013, 07	11 October, 07	44	0.3	−96	0.002	117	5	M1.5	1	...	360 M	1251 M

Table 1 (*Continued.*)

Solar event (UT)	SEP event (UT)	Flare–B (°)	I(B)	Flare–Earth (°)	I(Earth)	Flare–A (°)	I(A)	GOES X-Ray	Type III	Type II	CME dA (°)	CME V km s^{-1}
22 October 2013, 21	22 October, 22	141	0.002	00	0.01	−148	...	M4.2	1	...	360 M	658 M
25 October 2013, 08	25 October, 08	69	0.3	−73	0.001	139	...	X1.7	1	...	360 M	715 M
25 October 2013, 14	25 October, 15	74	1.0	−68	0.008	144	0.002	X2.1	1	...	360 M	1476 M
28 October 2013, 04	28 October, 04	−147	BG	71	0.04	−77	0.002	M5.1	1	...	50*	1180*
28 October 2013, 15	28 October, 16	114	0.2	−28	BG	−176	BG	M4.4	1	...	132*	589*
2 November 2013, 04	2 November, 04	−90	0.04	127	0.02	−21	1.5	...	1	...	360*	589*
4 November 2013, 05	4 November, 06	−49	BG	168	BG	20	1.2	...	1	...	134*	806*
6 November 2013, 23	7 November, 01	−118	BG	99	0.01	−50	BG	M1.8	1	...	360 M	1358 M
7 November 2013, 10	7 November, 10	0	12	−143	BG	68	1.3	...	1	...	360 M	1820 M
19 November 2013, 10	19 November, 11	−146	0.001	69	0.04	−80	0.0006	X1.0	1	...	360 M	959 M
26 November 2013, 15	26 November, 15	−44	...	169	...	20	0.0006	...	1	...	...	...
30 November 2013, 05	30 November, 06	−63	...	150	0.0009	0	0.0005	...	1	...	98*	371*
30 November 2013, 15	30 November, 15	0	0.0002	−146	BG	63	BG	...	0	...	140*	496*
5 December 2013, 10	5 December, 14	40	0.003	−108	BG	102	0.001	...	0	...	132*	422*
7 December 2013, 07	7 December, 09	−164	...	49	0.0004	−100	...	M1.2	1	...	132*	919*
9 December 2013, 19	9 December, 23	78	0.0005	−70	...	139	0.0003	C1.9	0	...	166*	606*
12 December 2013, 03	12 December, 04	−165	...	46	0.001	−104	...	C4.6	1	...	146*	672*
13 December 2013, 20	13 December, 20	0	...	−149	...	61	0.001	...	1	...	144*	456*
14 December 2013, 02	14 December, 02	3	...	−146	...	64	0.006	...	1	...	...	...
14 December 2013, 06	14 December, 06	5	...	−144	0.002	66	0.02	...	1	...	72*	644*
16 December 2013, 21	16 December, 22	−101	...	110	0.0002	−40	...	C3.1	1	...	102*	508*

Table 1 (*Continued.*)

Solar event (UT)	SEP event (UT)	Flare–B (°)	I(B)	Flare–Earth (°)	I(Earth)	Flare–A (°)	I(A)	GOES X-Ray	Type III	Type II	CME dA (°)	CME V km s^{-1}
26 December 2013, 03	26 December, 04	−10	0.8	−161	0.03	49	0.8	...	1	...	202*	856*
28 December 2013, 17	28 December, 18	−78	BG	130	0.3	−20	BG	...	1	...	218*	1420*

Column 1: Date, hour of solar event; Column 2: Date, hour of SEP onset at spacecraft with earliest onset; Column 3: Longitude of solar event relative to STEREO B where positive (negative) indicates that the event is west (east) of the spacecraft; Column 4: ∼25 MeV proton intensity ((MeV s cm^2 sr)$^{-1}$) at STEREO B. '...' indicates that the SEP event was not detected above $\sim 10^{-4}$ (MeV s cm^2 sr)$^{-1}$, and 'BG' that a high background from a previous event may have obscured the onset; Column 5: Longitude of solar event relative to Earth/SOHO; Column 6: ∼25 MeV proton intensity at Earth/SOHO; Column 7: Longitude of solar event relative to STEREO A; Column 8: ∼25 MeV proton intensity at STEREO A; Column 9: GOES soft X-ray flare intensity; Column 10: Type III radio emissions observed by WIND/WAVES or STEREO A/B SWAVES (0 = no; 1 = yes); Column 11: Type II emissions observed by WIND/WAVES or STEREO A/B SWAVES (0 = no; 1 = yes; 2 = "IP" type II extending below 1 MHz; available to May 2013 at the time of writing); Column 12: CME width, and Column 13: CME speed. The CME parameters are from the CUA/GSFC/CDAW LASCO catalog (available to May 2013 at the time of writing) except where indicated by '*' = from the CACTUS LASCO catalog, 'M' = from the real-time LASCO halo CME reports, 'A' = from the CACTUS STEREO A catalog, and 'B' = from the CACTUS STEREO B catalog.

estimated within the first 24 hours or so of the event, so that a higher peak in association with passage of an interplanetary shock (generally rare at these energies) is not taken as the "peak" of the event. In some cases, a slowly rising, extended particle event is observed without an *in-situ* shock, and peak intensity may be estimated at a later time. "BG" indicates that there is a high background from a preceding event that might obscure the event at that spacecraft, while "..." means that the event was not detected at $\sim$25 MeV above a threshold of $\sim 10^{-4}$ (MeV s cm^2 sr)$^{-1}$.

The following column shows the GOES soft (1 – 8 Å) X-ray flare intensity, for front-side or near-limb events. The presence of type III radio emissions below 20 MHz in the daily summary plots of WIND/WAVES or STEREO/SWAVES data is indicated by '1' in the next column, similarly in the next column for an event in the list of "possible" type II emissions observed by WIND/WAVES or STEREO/SWAVES. As discussed by Cane and Erickson (2005), many of the type II radio events in this list are minor, do not last for very long and cover a limited frequency range, indicating that the associated shocks are not particularly strong, whereas strong interplanetary shocks typically produce broad-band radio emissions ("IP type II events"; Cane *et al.*, 1982; Cane and Stone, 1984; Cane, 1985) starting below a few MHz. Thus, if the type II emissions extended below 1 MHz, indicative of an IP type II event, this is denoted by '2' and not by '1'. At the time of writing, the type II event list was only available up to May 2013.

The next two columns give the angular width and speed of the associated CME. For consistency with our previous studies (*e.g.*, Cane, Richardson, and von Rosenvinge, 2010a), we show CME widths and speeds from the Catholic University of America/Goddard Space Flight Center CDAW CME catalog (http://cdaw.gsfc.nasa.gov/CME_list/; Yashiro *et al.*, 2004) compiled from observations made by the LASCO coronagraphs on SOHO, while recognizing that SOHO may not be the best spacecraft (*e.g.*, closest to quadrature) to observe the CME speed and width with minimal plane of the sky projection. Since these values were only available until May 2013 at the time of writing, values from the CACTUS LASCO CME database (http://sidc.oma.be/cactus/), indicated by an asterisk, or from the SOHO real-time observer e-mail halo CME alerts (http://umbra.nascom.nasa.gov/lasco/observations/halo/soho-halo-alerts/), indicated by 'M', are included for more recent events. In a few cases where there are no LASCO observations, CACTUS CME widths and speeds from STEREO A or B are listed, indicated by 'A' or 'B', respectively. Data gaps are indicated by "DG".

2.2. Example Events

Table 1 indicates that individual SEP events were observed by just one spacecraft, or by two or three. (While the number of observing spacecraft does of course depend on the spacecraft locations relative to the solar event as well as on the longitudinal extent of the SEP event, we show below that this parameter orders the SEP properties to some degree.) Figure 4 shows two of the most intense probable single-spacecraft proton events, on 9 and 11 May 2011. The first was associated with a solar event at $\sim$21 UT on 9 May near central meridian with respect to STEREO B, which observed the particle enhancement, and at E94° (*i.e.* just behind the east limb) as viewed from Earth. The locations of STEREO A and B and Earth with respect to the solar event are shown below the data panel. Nominal Parker spiral field lines are drawn to the Sun using the observed solar-wind speed at each location. A C5.4 X-ray flare and a fast (1318 km s^{-1}) and wide (292°) CME (values from LASCO) were observed, together with IP type II and type III radio emissions. The 14 – 24 MeV proton intensities at STEREO A (for which the solar event was at W174°) and SOHO suggest that

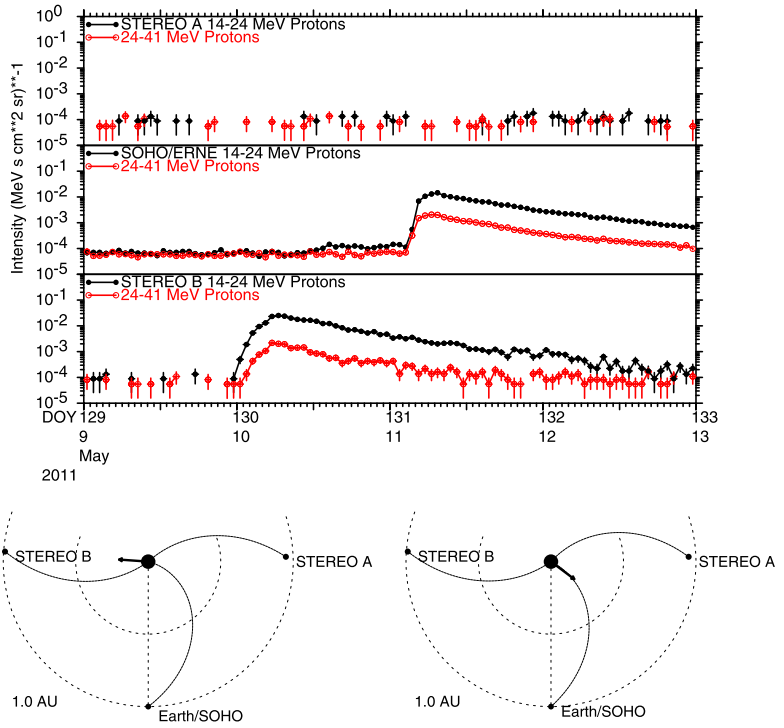

Figure 4 Intensities of protons at 14 – 24 MeV (black) and 24 – 41 MeV (red) observed by the HET instruments on STEREO A and B (top and bottom data panels, respectively) and the ERNE instrument on SOHO (middle panel), for two one-spacecraft events in May 2011 from two different active regions. The locations of the spacecraft relative to the solar events are shown below. Nominal Parker spiral magnetic field lines passing each spacecraft are indicated. In both cases, the particle event is observed at the spacecraft that is best connected to the solar event.

this event may just have been detected at these spacecraft, but at $\sim$25 MeV, the intensity did not increase above our threshold of $\sim 10^{-4}$ (MeV s cm^2 s)$^{-1}$.

The second SEP event in Figure 4, detected by ERNE, was associated with a solar event at $\sim$02 UT on 11 May at W53° with respect to Earth, which was nominally well-connected to the solar event by the IMF. The event was at E33° with respect to STEREO A, which showed no significant increase of $\sim$25 MeV protons, and at W147° with respect to STEREO B, where it is possible that the decay of the preceding event might have obscured a weak enhancement from this event. A B8.1 X-ray flare and a 745 km s^{-1} LASCO CME with a width of 225° were associated with the particle event, as well as type III radio emissions (occulted at STEREO B, as might be expected), but no reported type II. Thus, both these single-spacecraft particle events were associated with wide and reasonably fast CMEs (in one case, exceeding 1000 km s^{-1}), and the particle event was only detected by the spacecraft that was best connected to the solar event.

Figure 5 shows an example of a three-spacecraft SEP event that occurred early on 21 March 2011. The solar event was observed by STEREO A at approximately W50° with respect to this spacecraft, which was well-connected to the event and observed a prompt increase in particle intensity. The HET observed the 0.7 – 4 MeV electron onset at 02:33 UT $\pm$ 1 minute. (HET electron intensities in this and other event figures are corrected as dis-

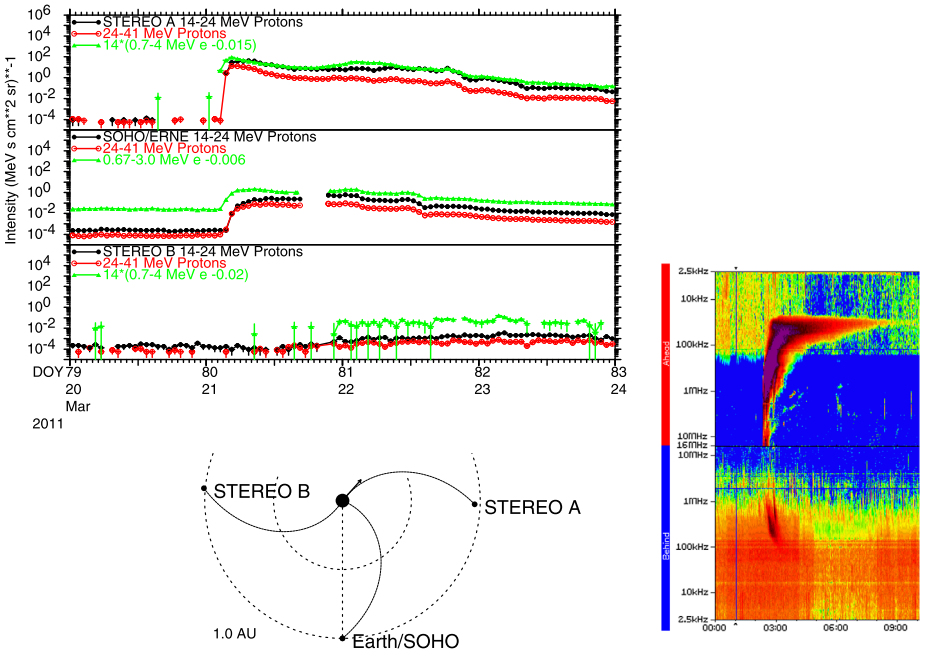

Figure 5 A three-spacecraft event on 21 March 2011. Intensities of 14 – 24 and 24 – 41 MeV protons and 0.7 – 4 MeV electrons (corrected for background and the HET calibration error) observed by the STEREO A and B HETs are shown in the top and bottom panels, respectively. The middle panel shows proton intensities at the same energies from the ERNE instrument on SOHO and the 0.67 – 3 MeV electron intensity from EPHIN. The particle event rose most promptly, and was most intense, at STEREO A, which was best connected to the solar event, whereas a delayed rise and weak event, barely above background, was observed at STEREO B, which was connected $\sim 170^\circ$ from the solar event. Though the event was on the far side of the Sun (W138°) relative to Earth, a clear, reasonably prompt event onset was observed by ERNE. Particle intensities were around two orders of magnitude lower than at STEREO A. The right-hand panel shows 2.5 kHz – 16 MHz radio observations from STEREO A (top) and B (bottom) in a "mirrored" format, illustrating the bright, long-duration type III emissions that accompanied this event. The occultation at high frequencies at STEREO B (and also WIND, not shown) by the limb of the Sun is consistent with the spacecraft locations with respect to the solar event. Slower drifting type II emission is also evident at STEREO A at 02:30 – 04:30 UT.

cussed above in relation to Figures 3(f) and (g).) The electron onset occurred ~ 13 minutes after the onset of bright, long-duration type III radio emissions observed by STEREO A SWAVES at 02:20 UT; see the right-hand panel in Figure 5. The emissions were occulted at high frequencies by the limb of the Sun when observed at STEREO B (and also at WIND, not shown), consistent with the configuration of the spacecraft relative to the solar event shown in Figure 5. Interplanetary type II radio emission was also observed by STEREO A at 02:30 – 04:30 UT. HET A observed the 24 – 41 MeV proton intensity increase from 03:14 UT ± 2 minutes, *i.e.* ~ 40 minutes later than the near-relativistic electron onset. A 25 MeV (40 MeV) proton would take ~ 45 (35) minutes to travel from the Sun along a nominal 1.2 AU spiral magnetic-field line, suggesting that this delay may be largely accounted for by the proton propagation time from the Sun. The solar event was at W138° relative to Earth. Nevertheless, a reasonably prompt particle increase was also observed (0.67 – 3 MeV electron and 24 – 41 MeV proton onsets were at 03:14 UT ± 5 minutes and 03:40 UT ± 5 minutes, respectively). However, the particle intensities were around

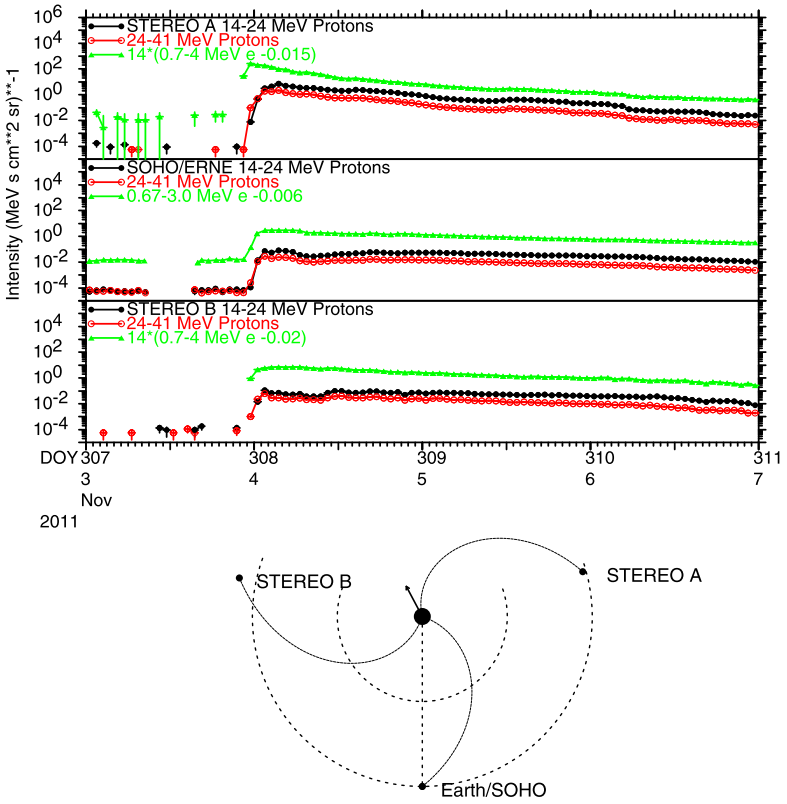

Figure 6 A three-spacecraft event on 3 November 2011 in which the particle intensity rose promptly at all three spacecraft, including at Earth, for which the solar event was at E152°. Again note that the event was most intense at the best-connected spacecraft, STEREO A.

two orders of magnitude lower than at STEREO A. The event was at E127° with respect to STEREO B, which was connected to the Sun ∼170° from the event. HET B observed a weak, slowly rising increase that we attribute to this event. Proton intensities were another ∼two orders of magnitude lower than at Earth. Thus, the particle event was most prompt and most intense at the best-connected spacecraft, and the onset delay increased and the intensity decreased as the spacecraft connection to the event became weaker. The associated CME had a mean speed of 833 km s^{-1} and width of 260° based on CACTUS analysis of observations from STEREO B, the spacecraft closest to quadrature, while the LASCO CDAW catalog classifies this as a full-halo CME with a speed of 1341 km s^{-1}. See Rouillard *et al.* (2012) for a detailed study of the relationship between the solar eruption, CME and energetic particle onset of this event.

The three-spacecraft event late on 3 November 2011 (Figure 6) was remarkable in that the proton and electron intensities showed relatively prompt increases at all three spacecraft despite their wide separation. STEREO B observations show that the associated solar event was at ∼50° east of this spacecraft. The particle event was again most intense at the best-connected spacecraft (STEREO A) and was around two orders of magnitude weaker at the other spacecraft. Figure 7 shows an expanded view of the beginning of the event using one-minute averaged data from the STEREO HETs and five-minute averaged ERNE and EPHIN

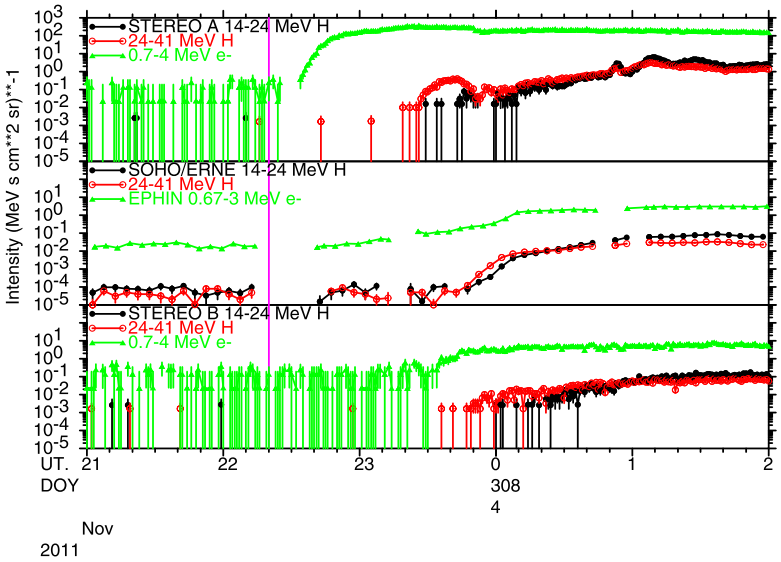

Figure 7 Expanded view of the onset of the event on 3 November 2011, showing one-minute averaged data from the STEREO HETs, and five-minute averaged data from SOHO ERNE and EPHIN. The vertical line indicates the onset time of type III radio emissions observed by STEREO A SWAVES. Electrons were first detected at STEREO A around 13 minutes after this time, followed by 24 – 41 MeV protons 52 minutes later. Similar energy protons arrived at STEREO B and Earth with an additional delay of ∼25 minutes.

observations. The electron onset occurred at STEREO A at 22:33 UT, around 13 minutes after the beginning of the associated type III emissions (interplanetary type II emissions were also observed by STEREOs A and B starting at 22:35 UT). The 24 – 41 MeV proton intensity at STEREO A increased around 52 minutes later. The proton intensity increased at Earth around 25 minutes later, and at a similar time at STEREO B. Thus, within 25 minutes after protons were detected at the best-connected spacecraft, they were also detected at the other two poorly connected spacecraft. Dividing the angular distance between the footpoints of the field lines to STEREO A and SOHO by 25 minutes suggests an angular propagation speed of 5.3°/minute, corresponding to a speed of 1070 km s^{-1} at the surface of the Sun. This turns out to be reasonably similar to the expansion speed of the associated LASCO CME (991 km s^{-1}) given in the CUA/GSFC catalog, although this may be fortuitous (see the discussion of Figure 17 below). This was also a full-halo CME. CACTUS CME speed estimates are 625 km s^{-1} (LASCO), 781 km s^{-1} (STEREO A, closest to quadrature) or 694 km s^{-1} (STEREO B). We note that despite the widespread, relatively prompt onset, this particle event was not associated with an especially fast CME. The CME speed is, for instance, similar to the speeds of the CMEs associated with the single-spacecraft events in Figure 4. We also examined the possibility that two or more solar events were involved in this widespread particle event, such as sympathetic flares (Richardson, 1936; Moon *et al.*, 2002; Schrijver and Title, 2011; Schrijver *et al.*, 2013) triggered by the initial event. However, solar imaging, WAVES/SWAVES radio observations, X-rays and other observations show no evidence that multiple events were involved. In particular, an X1.9 flare at E63° relative to Earth with peak intensity at 20:27 UT, around two hours earlier, played no role since STEREO B was well-connected to this flare and did not detect any particle increase. In addition, there were no type II or type III radio emissions associated with this flare, and the

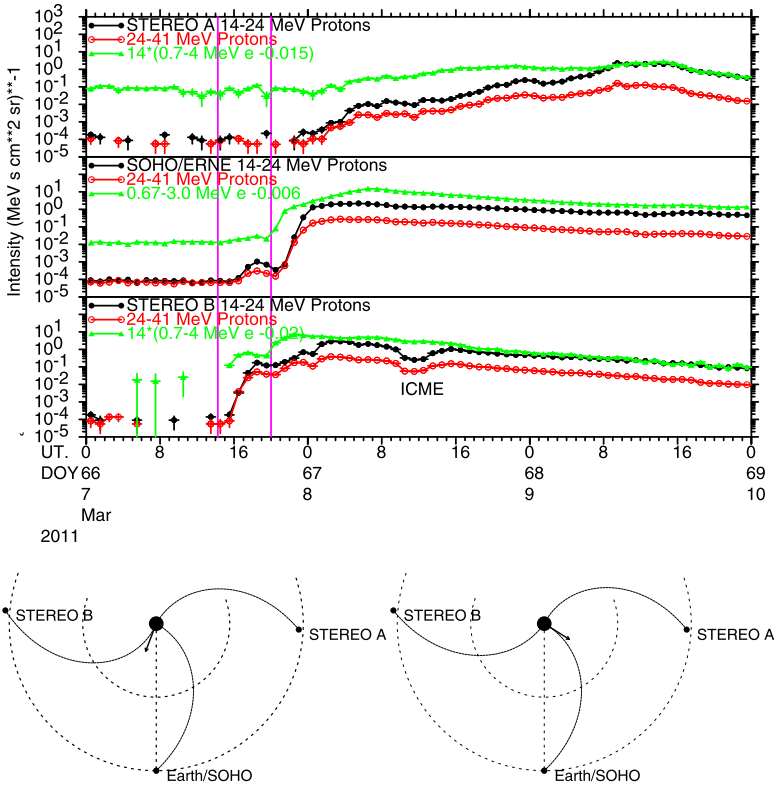

Figure 8 Observations for two particle events from different active regions on 7 March 2011. Vertical lines give the onset times of type III radio emissions. The first event, from E21° (relative to Earth), was most prominent at STEREO B, the best-connected spacecraft. The second, from W53°, was best connected to Earth, but was also observed at the other spacecraft. At STEREO A, the intensity peaks at passage of the shock on 9 March that was probably associated with this event.

STEREO B COR 1 coronagraph only observed a narrow ($\sim 30°$ width) CME that does not appear in the CDAW or CACTUS catalogs.

Particle increases associated with closely timed solar events do occur occasionally, and consideration of the solar, radio and particle data together can typically lead to a plausible interpretation. For example, two particle onsets from different active regions occurred within seven hours on 7 March 2011 (Figure 8). The first was associated with an M1.9 flare at E21° relative to Earth, accompanied by a 698 km s^{-1} partial halo CME (LASCO/CUA) and was most intense at STEREO B, which was well-connected to the event. A weak increase was seen at Earth, while there is no clear evidence of an increase at STEREO A. Type III radio emissions commenced at 14:15 UT, while type II emission was observed at STEREO B and WIND from 14:30 UT. A second solar event was associated with an M3.7 flare located at W53° relative to Earth and a fast (2125 km s^{-1}) halo CME that was best connected to Earth, where SOHO observed a large prompt onset. STEREO A, for which the event was at E35°, observed a more slowly rising particle enhancement, peaking at a shock that passed the spacecraft on 9 March, which was probably associated with the same solar event/CME. Such a profile is typical of an eastern event (*cf.*, Cane, Reames, and von Rosenvinge, 1988). Electron observations suggest that STEREO B also detected particles

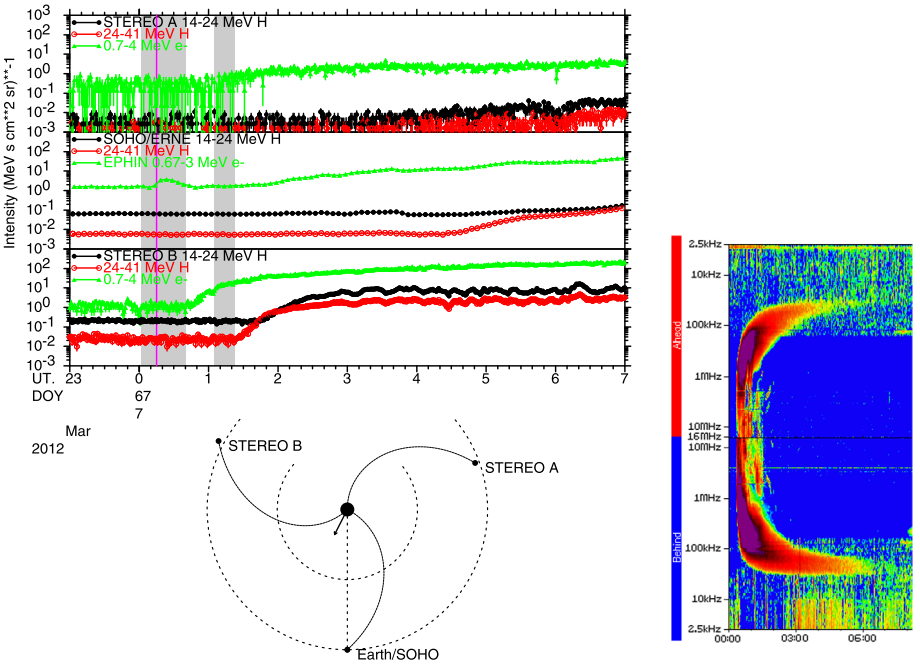

Figure 9 Observations of the onset of the 7 March 2012 particle event. Shaded regions indicate the durations of two X-class X-ray flares at E27° (also evident as contamination in the EPHIN electron channel) and E17° relative to Earth, both accompanied by fast halo CMEs. The vertical line gives the onset time of the bright type III emissions observed by STEREO A and B (right panel) and at Earth that accompanied the first event. Observations at STEREO B (1 minute averages) clearly demonstrate that the onset of particle acceleration was associated with the first event and not with the second; there is no additional feature in the intensity–time profile that might be related to the second event.

from this event, and they probably also contributed to the proton enhancement. However, the intensity profile at STEREO B is complicated by the passage of a shock, sheath, and interplanetary coronal mass ejection (ICME) on 7 – 8 March. In particular, the brief intensity decrease on 8 March is associated with passage of the ICME. In this region, Leske *et al.* (2013) reported field-aligned bidirectional ∼5 MeV proton flows, characteristic of ICMEs (*e.g.*, Zurbuchen and Richardson (2006) and references therein). This second particle event was associated with bright, long-duration type III radio emissions (occulted at STEREO B) commencing at 20:00 UT and IP type II emission from 20:00 UT observed by STEREO A and WIND.

Our final example, which occurred one year after the previous event, is a case where two CMEs erupted in the vicinity of AR 1429 separated by ∼one hour. On 7 March 2012, an X5.4 flare (onset: 00:02 UT; peak: 00:24 UT; end: 00:40 UT) at E27° with 3B Hα emission was followed by an X1.3 flare (onset: 01:05 UT; peak: 01:14 UT; end: 01:23 UT) at E17°. Two fast halo LASCO CMEs were associated with these events, first observed above the occulting disk at 00:24 UT (with a speed of 2684 km s^{-1}), and at 01:30 UT (1825 km s^{-1}). Figure 9 shows one-minute averaged observations from the STEREO HETs and five-minute averaged SOHO ERNE and EPHIN data during the onset of this event. The electron intensity at STEREO B, the best-connected spacecraft, was clearly increasing by ∼00:45 UT. As is typical (*cf.*, the events described above, and further discussion below), proton onset was delayed by ∼40 minutes, to ∼01:25 UT. These onset times are clearly consistent with an

association with the first solar event (shaded regions indicate the X-ray flare intervals for the two events) and are inconsistent with an association with the second solar event. While the particle event was eventually observed at the other spacecraft, note that the well-connected STEREO B observations provide unambiguous evidence of the correct solar association. We also note that only the first event was accompanied by bright type III radio emissions, again consistent with this being the site of particle acceleration and release. Interplanetary type II emission commenced at 01:00 UT, also ahead of the second event.

The occurrence of these two closely spaced CMEs might be expected to be an ideal situation for particle acceleration by multiple shocks to take place (*e.g.*, Pomerantz and Duggal, 1974; Levy, Duggal, and Pomerantz, 1976; Cliver and Kallenrode, 2001) or multiple CMEs (*e.g.*, Gopalswamy *et al.*, 2002, 2004; Li *et al.*, 2012). We note that Cliver and Kallenrode (2001) concluded that acceleration by multiple shocks does not necessarily require the shocks to be converging, so the fact that the first CME was faster than the second according to the CDAW LASCO CME database would not necessarily rule out this process from occurring. It has also been suggested that a preceding CME may provide a "seed" population for acceleration by the shock of a second CME, or may in some way "precondition" the solar wind through which the second CME shock travels to promote particle acceleration. However, the observations of this particle event onset clearly indicate that particle acceleration was associated with the first solar event/CME and that the second CME was not involved. In addition, there is no obvious indication in the STEREO B intensity–time profile of a second particle injection associated with the second solar event. This, together with the absence of type III emissions (as discussed above and also below, the vast majority of > 25 MeV proton events are accompanied by such emissions) also suggest that the second solar event played no role in particle acceleration near the Sun.

3. Summary of SEP Events

3.1. Occurrence Rate

Figure 10 summarizes the occurrence of > 25 MeV proton events *at Earth* from 1996 to December 2013, updated from Cane, Richardson, and von Rosenvinge (2010a) and Cane, Richardson, and von Rosenvinge (2010b). The top panel shows the event peak intensity at ~ 25 MeV. The second panel gives the number of SEP events/Carrington rotation and the three-rotation running mean (red), while the third panel shows the monthly sunspot number. The SEP event rate clearly tends to follow solar activity levels through Cycle 23 (though with SEP events persisting until well into the declining phase), the subsequent extended solar minimum, and into Cycle 24. The sunspot number in Cycle 24 reached a peak of 97 in November 2011 dominated by northern-hemisphere sunspots (Chowdhury, Choudhary, and Gosain, 2013), well below the maximum in Cycle 23, and then declined to around 60 for much of 2012 – 2013. Consistent with the decrease in the level of solar activity, the SEP rate declined from around mid-2012 into 2013, though fairly intense events were still observed occasionally, in particular in April – May 2013. Toward the end of 2013, the sunspot number (now dominated by southern-hemisphere sunspots) appears to increase once again, and a corresponding increase in the SEP rate is also evident. We therefore suggest that the decline in activity in 2012 – 2013 is an example of the temporary decrease in energetic solar activity, including SEP events, often termed the Gnevyshev gap, which is frequently found near solar cycle maxima (*e.g.*, Gnevyshev, 1967, 1977; Feminella and Storini, 1997; Storini *et al.*, 2003; Bazilevskaya, Makhmutova, and Sladkova, 2006; Norton and Gallagher, 2010; Richardson and Cane, 2012, and references therein).

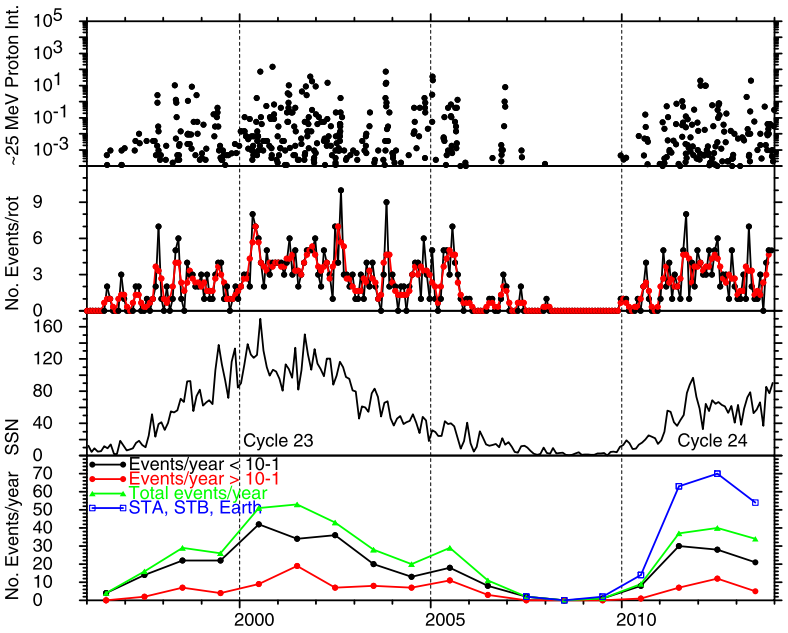

Figure 10 Summary of the rate of > 25 MeV proton events at Earth during January 1996 – December 2013. The top panel shows the event peak intensity at ∼25 MeV (in $(\text{MeV s cm}^2\text{ sr})^{-1}$), while the second panel gives the number of events/Carrington rotation with intensities $> \sim 2 \times 10^{-4}$ $(\text{MeV s cm}^2\text{ sr})^{-1}$ and the three-rotation running mean (red graph). The monthly sunspot number is shown in panel three. Panel four gives the yearly number of events at Earth (green) and those with intensities above (red) or below (black) 0.1 $(\text{MeV s cm}^2\text{ sr})^{-1}$. The blue graph shows the number of individual events identified at STEREO A or B, or at Earth.

An interesting difference between Cycles 23 and 24 is that 25 MeV proton events were present in Cycle 23 from around two months after the time of sunspot minimum in May 1996, whereas the first event at Earth in Cycle 24 was detected with a delay of a year after sunspot minimum, which occurred in December 2008. The SEP occurrence rate (second panel) then rose somewhat more rapidly than during the rise of Cycle 23. The yearly SEP event rates at Earth (bottom panel) appear to have been reasonably similar in the two cycles based on the observations so far, being only ∼20 % below the highest rates in Cycle 23. However, the yearly rates for 2013 indicate a decline from the previous year. The blue graph in the bottom panel shows the number of individual events (as in Table 1) observed at STEREO A or B or at Earth. Around 30 % of these events were not detected at Earth. Again there is an indication of a decrease in the SEP event rate in 2013 by around a third from the rate in 2012.

3.2. Solar Event Properties

When discussing the properties of SEP events at the STEREO spacecraft and at Earth and the associated solar events, we generally focus on the subset of events detected from December 2009 when the STEREO spacecraft were ≥ 65° from Earth and the SEP rate increased in Cycle 24, to December 2012, when the STEREO spacecraft were separated by 99° on the far side of the Sun. Although the spacecraft constellation was changing during this period,

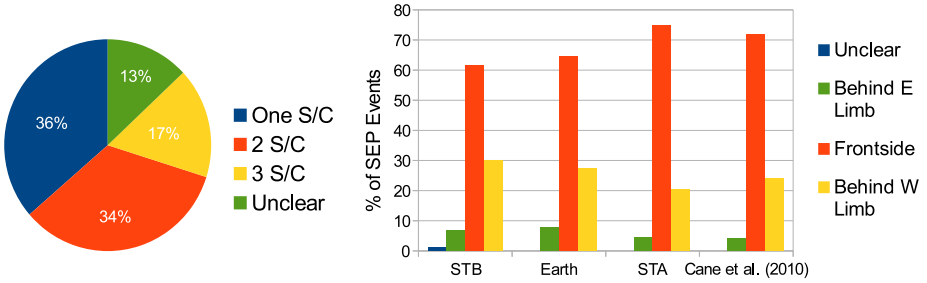

Figure 11 The left-hand panel shows the distribution of > 25 MeV proton events detected by one, two, or three spacecraft, and those for which the number of detecting spacecraft is unclear, from December 2009, when the STEREO spacecraft were $\sim 65°$ from the Sun–Earth line, to December 2012, when the STEREO spacecraft were separated by 99°. The right-hand panel shows the percentages of events that originated behind the east limb, on the front side of the Sun, or behind the west limb, relative to STEREO B, Earth, or STEREO A, and for the events in 1997 – 2006 discussed by Cane, Richardson and von Rosenvinge (2010a).

the spacecraft were well separated, with the STEREO spacecraft positioned approximately above the limbs of the Sun as observed from Earth. The left-hand panel of Figure 11 shows the percentages of the ~ 25 MeV proton events during this interval that were detected by only one, only two, or all three spacecraft. For 13 % of the events, the number of observing spacecraft is unclear because of data gaps or high background from preceding events. Otherwise, 36 % of the SEP events were observed by only one spacecraft, 34 % at only two spacecraft, and 17 % at all three spacecraft. (Considering all the events in Table 1, 36 % were observed by one spacecraft, 34 % by two spacecraft, and 21 % by all three.) As we discuss below, the number of spacecraft that detected an SEP event, which gives a crude indication of the longitudinal extent of the event, but is appropriate for this study, which focuses on identifying events at the different spacecraft, does tend to organize the event properties. The right-hand panel summarizes the percentage of events that originated behind the east or west limbs, or on the front side of the Sun from the viewpoint of STEREO A, B, or Earth. Before the STEREO spacecraft approached the limbs of the Sun, which allowed observations of the far side of the Sun, the detection at Earth of SEP events originating behind the limbs of the Sun could only be inferred indirectly, for example, from CMEs originating behind the limb, occulted type III radio emissions, and the presence of major active regions that had previously rotated across the west limb, or later emerged over the east limb. Thus, this panel also shows similar results based on the events detected during 1997 – 2006 at Earth in Cane, Richardson, and von Rosenvinge (2010a). The distribution of events is similar in each case, with $\sim 60 - 75$ % originating on the front side, $\sim 20 - 30$ % behind the west limb, and $\sim 4 - 8$ % behind the east limb. The east–west asymmetry reflects the favored connection to the western hemisphere of the Sun by the spiral interplanetary magnetic field.

Figure 12 shows the ~ 25 MeV proton intensity (including observations from all three spacecraft) plotted against the longitude of the solar event with respect to the observing spacecraft for events from December 2009 to, in this case, December 2013, providing a summary of all but the few earliest events in the study period. The symbol/color indicates the number of spacecraft that observed each event; 325 observations are included in the figure. One-spacecraft events (green crosses) predominantly originate on the western hemisphere, and typically have peak intensities $< 10^{-2}$ $(\mathrm{MeV\,s\,cm^2\,sr})^{-1}$. Thus, they are typically weaker events that are detected when a spacecraft is favorably connected to the event. Two-spacecraft events (red circles) are around two orders of magnitude more intense than single-spacecraft events at well-connected longitudes, and may originate from behind the

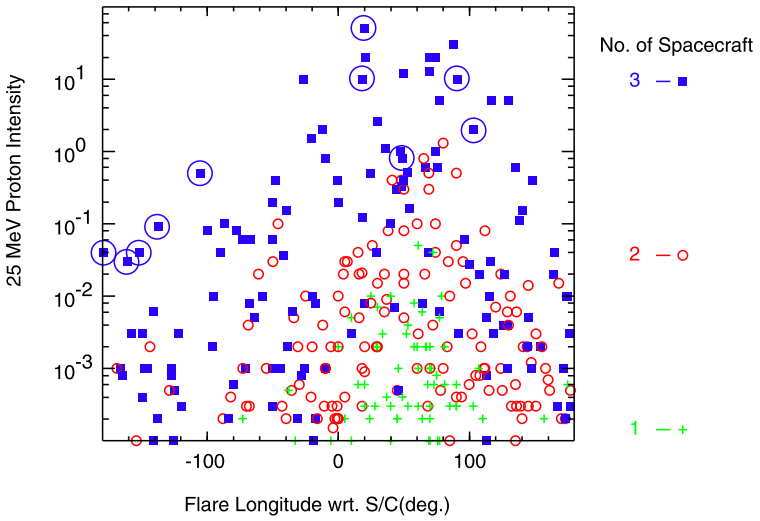

Figure 12 Peak intensities of ~25 MeV proton events (in (MeV s cm^2 sr)$^{-1}$) plotted against the longitude of the solar event relative to the observing spacecraft for events in December 2009 – December 2013, when the STEREO spacecraft were separated by > 58° in longitude. The symbol type indicates whether the event was detected at one (green cross), two (red circle) or three (blue square) spacecraft (a point is plotted for each observing spacecraft for multiple–spacecraft events). Three-spacecraft events with intensities higher than 10^{-2} (MeV s cm^2 sr)$^{-1}$ from behind the east limb are circled. The corresponding intensities at the best-connected spacecraft are similarly indicated.

west limb to the eastern front-side hemisphere. Three-spacecraft events typically have intensities around 1 – 2 orders of magnitude higher than two-spacecraft events and form the majority of events that are detected from behind the east limb. In particular, the five circled three-spacecraft events (22 September and 3 November 2011, 7 March and 23 July 2012, and 26 December 2013) had intensities > 10^{-2} (MeV s cm^2 sr)$^{-1}$ when observed by a spacecraft for which the event was behind the east limb. These were among the most intense events when observed by the best-connected spacecraft (also circled), suggesting that the intrinsic intensity of these events plays a role in their visibility at poorly connected spacecraft. On the other hand, it is also evident that three-spacecraft events have a wide range of intensities at well-connected longitudes and are not just the most intense. In particular, there are events ~3 orders of magnitude lower in intensity than the circled events that are also observed at all three spacecraft. An example is the 22 December 2009 event (Figure 13). The solar event, associated with a C7.2 flare at W46°, was well-connected to Earth, although interestingly, the proton event onset appears to have been more prompt at STEREO B, for which the event was just behind the west limb, than at Earth (both STEREO B and SOHO also detected electrons from this event). Type III radio emissions were observed at WIND and STEREOs A and B, and were occulted at STEREO B as expected. No type II emissions were reported. LASCO observed a slow (318 km s^{-1}), 47° width CME. Though the spacecraft separation was clearly smaller than in other three-spacecraft events discussed above and the event location was reasonably favorable for all three spacecraft, nevertheless, this event illustrates that even relatively weak events can be detected over a wide region of the inner heliosphere.

Figure 14 summarizes several relationships between the ~25 MeV proton peak intensity and properties of the associated solar events for events in December 2009 – December 2012. Table 1 indicates that every > 25 MeV proton event in this period had an associated CME,

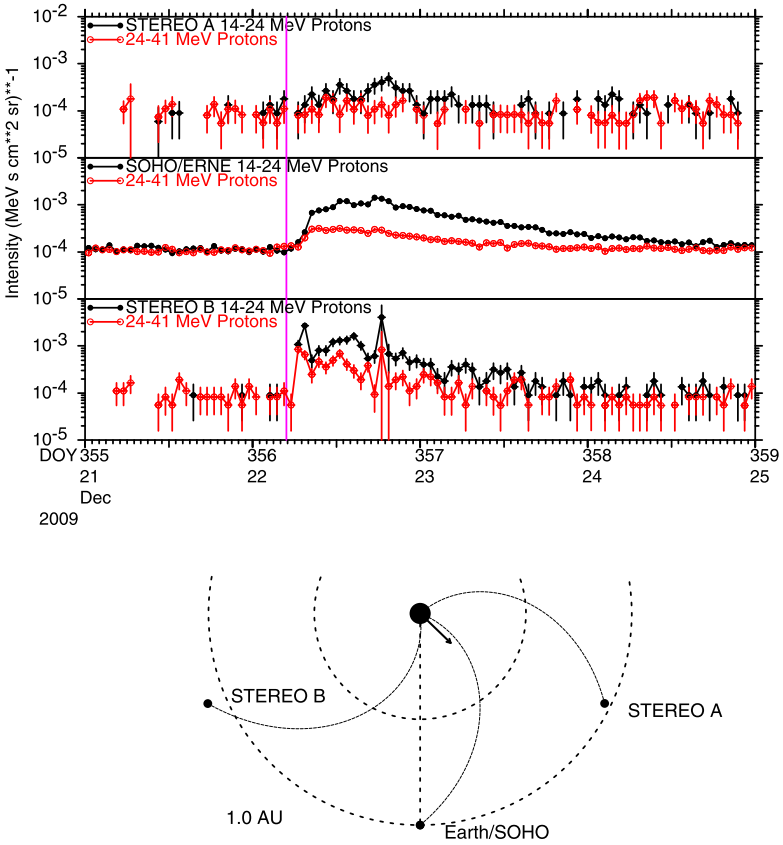

Figure 13 Observations of a weak three-spacecraft event on 22 December 2009. The vertical line gives the onset time of type III radio emissions (04:50 UT).

as also noted by Cane, Richardson, and von Rosenvinge (2010a) for similar events in Cycle 23. (A few late 2013 events do not have an assigned CME in the table, but only preliminary CME identifications were available at the time of writing.) The top-left panel of Figure 14 shows the proton intensity plotted against the speed of the LASCO CME for cases where the solar event is on the western front-side hemisphere (*i.e.*, W00 – 90°) relative to the observing spacecraft (STEREO A, B, or SOHO). The well-established correlation between proton intensity and CME speed is evident (*e.g.*, Kahler, Hildner, and Van Hollebeke, 1978; Kahler *et al.*, 1984; Kahler, 2001; Cane, Richardson, and von Rosenvinge, 2010a, and references therein). The symbol type indicates whether the proton event was detected at only one, only two, or at all three spacecraft. Single-spacecraft events tend to be associated with slower CMEs (below $\sim$1000 km s^{-1}), while the fastest CMEs in this sample tend to be associated with three-spacecraft events. Two-spacecraft events tend to have intermediate speeds. However, there are overlaps between the distributions. In particular, the three-spacecraft events extend to slower CMEs, even below 1000 km s^{-1}, so a fast CME is evidently not a requisite for an SEP event that is extended in longitude.

CME width may also be correlated with proton intensity (*e.g.*, Cane, Richardson, and von Rosenvinge, 2010a), but we have not examined this here for several reasons. As is

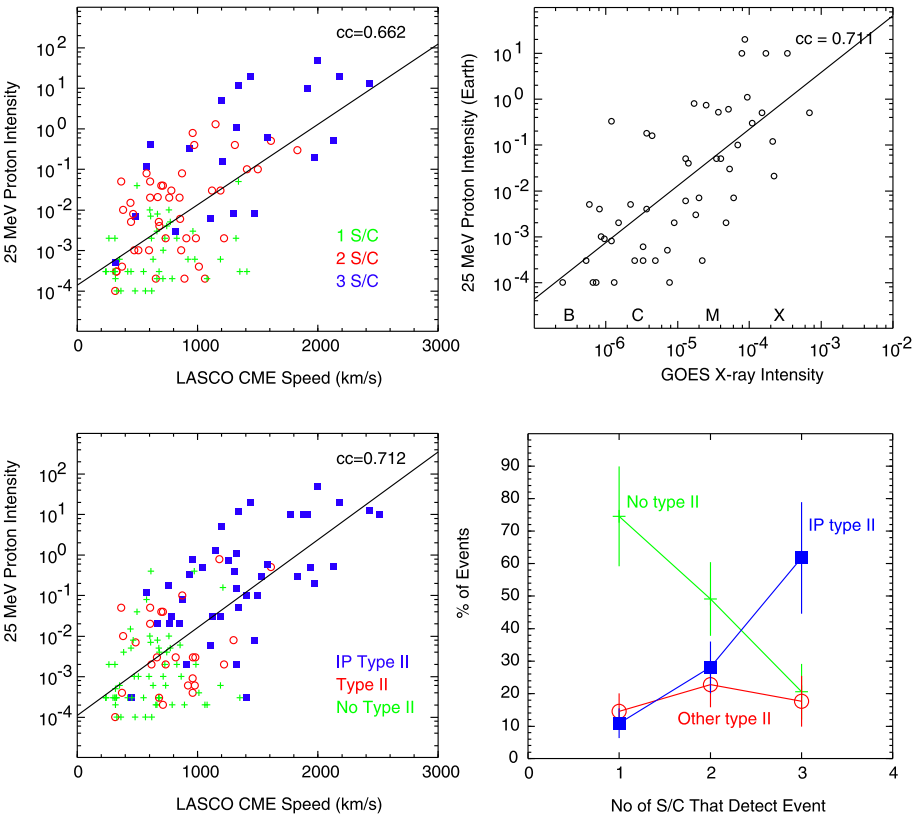

Figure 14 The top-left panel shows the ∼25 MeV proton intensity *versus* the speed of the associated LASCO CME, for cases in December 2009 – December 2012 where the solar event is on the western front-side hemisphere relative to the observing spacecraft. The symbol indicates whether a particle event was observed at one, two, or three spacecraft. The upper-right panel shows the proton intensity at Earth plotted *vs.* the GOES soft X-ray flare intensity for western-hemisphere events. The bottom-left panel shows the proton intensity *vs.* CME speed (as in the upper left, but including a few events for which the number of spacecraft is uncertain). Green crosses indicate that no WAVES type II radio emissions were reported, blue squares that IP type II emissions defined here as extending below 1 MHz were observed, and red circles that type II emissions were detected, but did not extend below 1 MHz. The bottom-right panel shows the percentage of events detected by one, two, or three spacecraft that were accompanied by no type II radio emissions, or by non-IP, or IP type II emissions.

evident from Table 1, around half (52 %) of the events (to May 2013) were associated with full-halo CMEs (360° width) in the CDAW LASCO CME catalog, *i.e.*, the ejection surrounds the coronagraph occulting disk. However, as discussed in Cane, Richardson, and von Rosenvinge (2010a), in many cases, such halo CMEs are highly asymmetric. In that article, halo-CME widths were reassessed by the authors, with only symmetric halo-CMEs retaining a width of 360°. While we would be able to do this for the current set of events, the resulting CME widths would still include projection effects. These could be reduced by obtaining the CME width (and also speed) from the spacecraft (STEREO or SOHO) that is closest to quadrature relative to the solar event. However, this will be the focus of a future study.

The top-right panel of Figure 14 shows the 25 MeV proton intensity plotted *vs.* the GOES soft X-ray flare peak intensity for events on the western hemisphere as observed from Earth. The proton and X-ray flare intensities are also correlated, with a correlation coefficient that is similar to that for the proton intensity correlation with CME speed, as also found for the 25 MeV proton events in Cycle 23 by Cane, Richardson, and von Rosenvinge (2010a). On the other hand, in the discussion above of the circumstances of the event in Figure 6, we noted that an earlier X1.9 flare was not accompanied by an SEP event. Including all 25 MeV proton events in this study for which an X-ray flare is listed in Table 1, 9 (7 %) of these flares were B class, 47 (37 %) were C class, 50 (40 %) were M class, and 20 (16 %) were X class. Thus, 77 % of these proton events were associated with C or M class flares.

In Table 1, 47 % of the events (up to May 2013) do not have possible type II emission observed by WIND/WAVES or SWAVES, 33 % are accompanied by IP type II events, defined here as emission that extends below 1 MHz, while the remaining 20 % have type II emissions that do not extend below this frequency. The bottom-left panel of Figure 14 shows the proton intensity *vs.* CME speed, again for western-hemisphere events at STEREO A, B, or SOHO, but in this case, the symbol indicates whether or not type II emission was reported, and whether this could be classified as IP type II. The absence of type II emission is evidently associated predominantly with low-intensity proton events (below $\sim 10^{-2}$ (MeV s cm^2 sr)$^{-1}$) with CME speeds below ~ 1000 km s^{-1}. Events with type II emission are fairly well separated into more intense events with faster CMEs that have IP type II emission, and those with other type II emission that have weak particle events and slower CMEs, with a distribution that significantly overlaps with the events without type II emission. Comparison with the top-left panel suggests that there might be some overlap between the events without type II emission and events detected at only one spacecraft, and similarly between three-spacecraft events and those with IP type II emission. The bottom-right panel in Figure 14 examines this in more detail, showing the percentage of events detected by one, two, or three spacecraft that were or were not accompanied by type II or IP type II emissions observed by WIND/WAVES or SWAVES. The results indicate that around three-quarters of single-spacecraft events were not accompanied by type II emission, compared with around 50 % of two-spacecraft events, and around 20 % of three-spacecraft events. Thus, the single-spacecraft events do indeed tend to lack reported type II emission. On the other hand, the fraction with IP type II emission rises from around 10 % for one-spacecraft events to around 30 % for two-spacecraft events, and around 60 % for three-spacecraft events. The fraction with other type II emissions only weakly depends on the number of detecting spacecraft and remains at $\sim 15-20$ %. In the conventional picture, where type II emissions are indicative of the formation of shocks, a possible interpretation is that shocks are absent from the majority of single-spacecraft events, but are more likely to be present in multiple-spacecraft events. Alternatively, it is possible that such emissions may be present in single-spacecraft events, but are too weak to be detected.

Examining the presence of type III radio emissions, 92 % of the events in Table 1 were accompanied by type III radio emissions, consistent with the high association between type III radio emission and SEP events noted by Cane, Erickson, and Prestage (2002) and Cane, Richardson, and von Rosenvinge (2010a). A possible interpretation of events without type III emissions is that these do not involve any flare-accelerated particles, only particles accelerated by the CME-driven shock, but a more detailed study of the individual events is required to investigate this possibility (for instance, the event of 24 February 2012, which is associated with an erupting filament; see also Cane *et al.*, 1986).

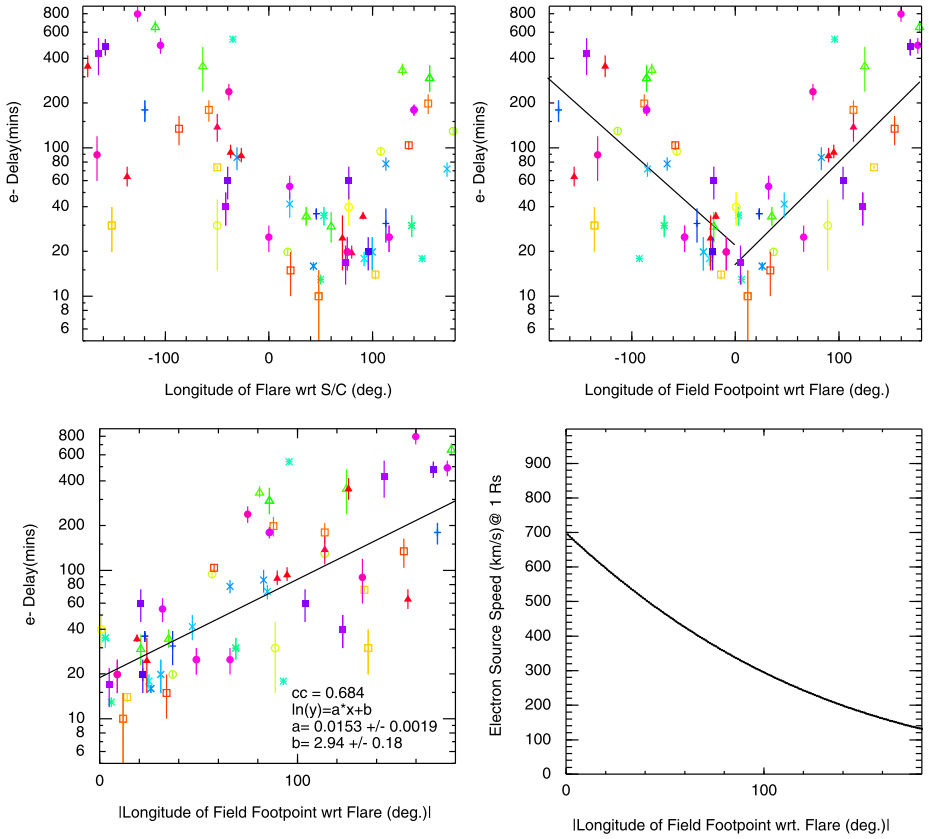

Figure 15 Summary of the ∼0.7 – 4 MeV electron onset delay *versus* solar-event location with respect to (wrt) the observing spacecraft (S/C; top left) and *versus* the angle between the footpoint of the field line passing the spacecraft and the solar event (connection angle; top right) for the three-spacecraft events in December 2009 – December 2012. Symbols indicate different events. Delays are typically shortest for western-hemisphere events when connection to the event is favorable. The fits to events with positive or negative connection angles suggest that delays are ∼ symmetric to the east and west of the solar event. The bottom-left panel shows the delay *vs.* the absolute connection angle. The delay at zero connection angle is $\sim 19 \pm 3$ minutes. The log-linear fit, if interpreted as increasing delays due to an electron source spreading in longitude at the surface of the Sun suggests propagation speeds in longitude shown in the bottom-right panel that decrease with distance from the event, from ∼700 km s^{-1} near the event to ∼130 km s^{-1} at 180° from the event.

3.3. Longitudinal Dependence of Three-Spacecraft SEP Events

3.3.1. Electron and Proton Delays to Onset at 1 AU

We now combine observations of the three-spacecraft SEP events in December 2009 to December 2012 to summarize the longitudinal dependence of several of their properties based on the ensemble of events. The top-left panel of Figure 15 shows the log of the ∼0.7 – 4 MeV electron onset delay (when this can be inferred) plotted *vs.* solar-event longitude with respect to the observing spacecraft. The electron onset time is estimated from inspection of intensity–time profiles using averaging intervals of one minute to one hour (for weak events with extended delays). The errors indicate the estimated accuracy to which the time when the

intensity significantly increases above fluctuations in the pre-event background can be inferred. The onset delays are measured relative to the start of the SWAVES or WIND/WAVES type III emissions as estimated from daily summary plots, since such emissions are observed for most events. Otherwise, the peak soft X-ray time is used. Symbols indicate observations of different events. Minimum delays are associated with western-hemisphere events that are expected to be better connected by the IMF to the observing spacecraft. To examine the influence of connection, the top-right panel shows the same observations plotted *versus* the connection angle (CA) between the footpoint at the Sun of the nominal spiral field line passing the spacecraft at the time of the event, calculated using the observed solar-wind speed at the spacecraft (Nolte and Roeloff, 1973) and the longitude of the solar event. A positive (negative) CA means that the footpoint lies west (east) of the solar event. (Note that this is the opposite convention to that used by Lario *et al.* (2013) in their study of SEP longitudinal intensity dependence that includes some of the same events.) Electron onset delays tend to be shortest for well-connected events. The fits to events with positive and negative connection angles suggest that typical delays are approximately symmetric about the event location. Thus, in the bottom-left panel, the electron onset delays are plotted *versus* |CA|. The fit indicates typical electron onset delays at 1 AU of ~ 19 minutes for CA $= 0°$ increasing to ~ 300 minutes (~ 5 hours) for CA $= 180°$, though longer delays are found in some events.

A simple interpretation of the results is that the onset delay at 1 AU is given by $\Delta t_o = t_I + t(\phi)$, where t_I includes the time for a particle to move from the Sun to the spacecraft, assumed to be approximately constant for each event, plus any other $\sim$event-independent delays relative to type III burst onset (for example in the acceleration process). The typical delay at zero connection angle gives an estimate of the typical value of t_I. The second term is an additional delay that increases with increasing connection angle ϕ at a typical rate that is indicated by the fitted line in the lower left panel of Figure 15. This delay might be ascribed to a source moving away from the solar event along the surface of the Sun (or at some other height) that injects particles onto the field line footpoints, after which they travel out to 1 AU. The slope of the fit in the lower left panel of Figure 15, which gives the rate of change in the delay as a function of connection angle, can be expressed as the propagation speed of the electron source shown in the bottom-right panel of Figure 15 *versus* longitude from the event. The speed is higher closer to the event because the rate of change in the delay time with connection angle is lower. It is also assumed that the source is moving on the solar surface. The results suggest a deceleration from ~ 700 km s^{-1} near the event to ~ 130 km s^{-1} at 180° from the event. For a source above the solar surface, the speeds would be multiplied by the source distance (in R_s) from the center of the Sun. In practice, the source motion may be more complex (for example, it may lie on an expanding three-dimensional shock), but this simple scenario at least gives an idea of the propagation speeds that might be implied by the observations with minimal interpretation. We also note that other studies (*e.g.*, Vainio *et al.*, 2013) have used a velocity dispersion analysis with observations of particles over a range of energies/speeds to infer the solar release times of the SEPs. We have not conducted such an analysis here because we considered only two proton and one electron energy ranges, which is insufficient for a reliable dispersion analysis, and we focused on the arrival time at 1 AU, which is most relevant for space-weather applications; we were not interested in the detailed timing of particle acceleration at the Sun.

Figure 16 shows similar results for the 14 – 24 MeV proton onset delay. The top-left panel shows that as for electrons, minimum delays occur for well-connected events on the western hemisphere relative to the observing spacecraft. The weighted fits in the top-right panel suggest an east–west asymmetry in the proton delays, with shorter delays for connection to the east of the event for large connection angles. However, a non-weighted fit is

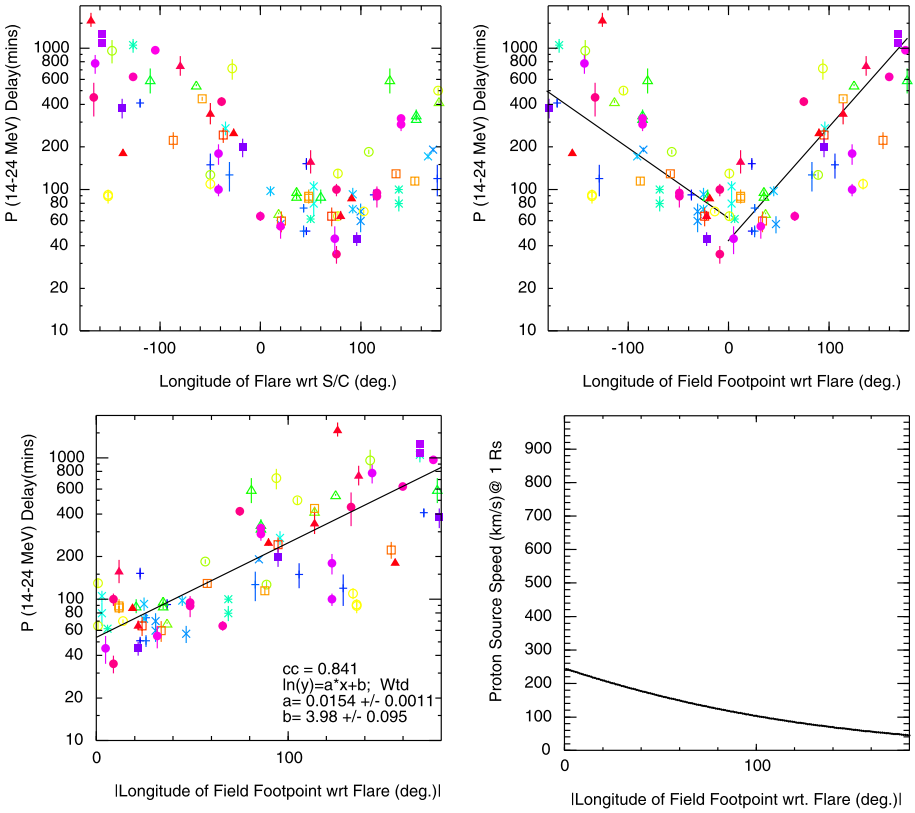

Figure 16 Summary plots of 14 – 24 MeV proton onset delays, in a similar format to Figure 15. Onset delays are again typically shortest for western-hemisphere events when connection to the event is favorable. The fits to events with positive or negative connection angles (top left) suggest some east–west asymmetry in the proton onset delay. However, plotting the delays *vs.* |CA| (lower left) indicates a typical delay at zero connection angle of ∼54 minutes. The slope of the log-linear fit is nearly identical to that for electrons. Thus, the ratio of the proton and electron onset delays is ∼constant at all connection angles. The source expansion speeds are slower than for electrons, ranging from ∼240 km s^{-1} near the event to 45 km s^{-1} at ∼180° from the event.

more symmetric. The bottom-left panel shows the correlation between the log of the proton onset delay and |CA|. The fit indicates that the typical delay at zero CA is 54 ± 5 minutes, increasing to $\sim 860 \pm 150$ minutes at $|\mathrm{CA}| = 180°$. Interestingly, the slopes of the fits in the bottom-left panels of Figures 15 and 16 are essentially identical (0.0153 ± 0.0019 compared with 0.0154 ± 0.0011), indicating that the ratio of the proton and electron onset delays derived from the fits is independent of connection angle, with a value of ∼2.8 that corresponds to the ratio of the proton and electron onset delays at CA = 0°. The ratio of electron and proton onset delays is discussed below; see also the *Helios* spacecraft results of Kallenrode (1993), which also indicate longer onset delays for protons than for electrons. The bottom-right panel of Figure 16 shows the proton source propagation speed inferred from the fit in the bottom-left panel. As for electrons, the source speed decreases with increasing longitude from the event, but the speeds are lower, from ∼240 km s^{-1} close to the event, to ∼45 km s^{-1} at CA = 180°, reflecting the longer proton onset delays.

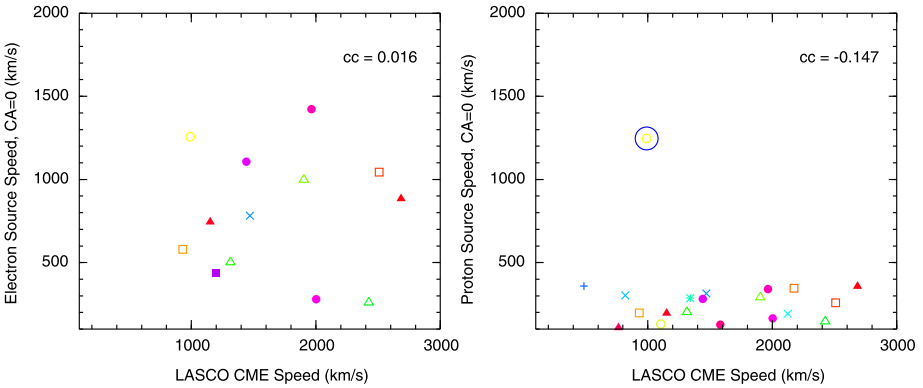

Figure 17 0.7 – 4 MeV electron (left) and 14 – 24 MeV proton source propagation speeds at zero CA inferred from |CA| *vs.* onset delays for individual events, plotted against the LASCO CME speed. The blue circle in the right-hand panel highlights the 3 November 2011 event.

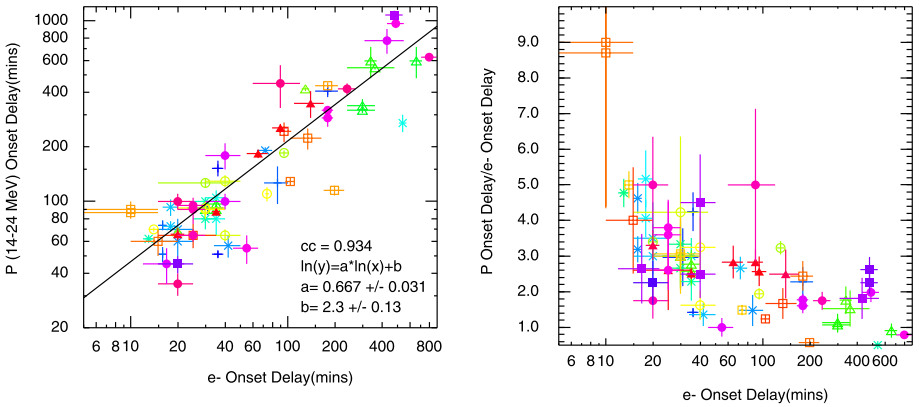

Figure 18 Left: correlation of the electron and proton onset delays for individual observations of the three--spacecraft events. Right: ratio of proton to electron onset delays as a function of electron onset delay.

Figure 17 examines whether there is any evidence of a correlation between the source propagation speeds at zero CA, inferred from fits to |CA| *versus* the log of the electron or proton onset delay *for individual events*, and the speed of the associated LASCO CME. The results indicate that there is little correlation, suggesting that the CME speed is a poor predictor of how rapidly particles spread out in longitude from the solar event, at least in this simple scenario. Note that the event with the outstanding high proton source speed (but not CME speed) circled in the right-hand panel is the 3 November 2011 event discussed above.

The left-hand panel of Figure 18 shows the log of the 14 – 24 MeV proton onset delay plotted against the log of the 0.7 – 4 MeV electron onset delay for the same event/spacecraft. These are highly correlated (cc = 0.934). However, the best fit indicates that $\Delta t_{oH} \sim 9.9\Delta t_{oe}^{0.67}$, implying that the $\Delta t_{oH}/\Delta t_{oe}$ ratio decreases with increasing onset delay and not the simple $\Delta t_{oH} \sim 2.8\Delta t_{oe}$ suggested by Figures 15 and 16. The right-hand panel of Figure 18 shows the ratio of the proton and electron onset delays for individual observations plotted against electron onset delay, illustrating the decline in the ratio with increasing delay,

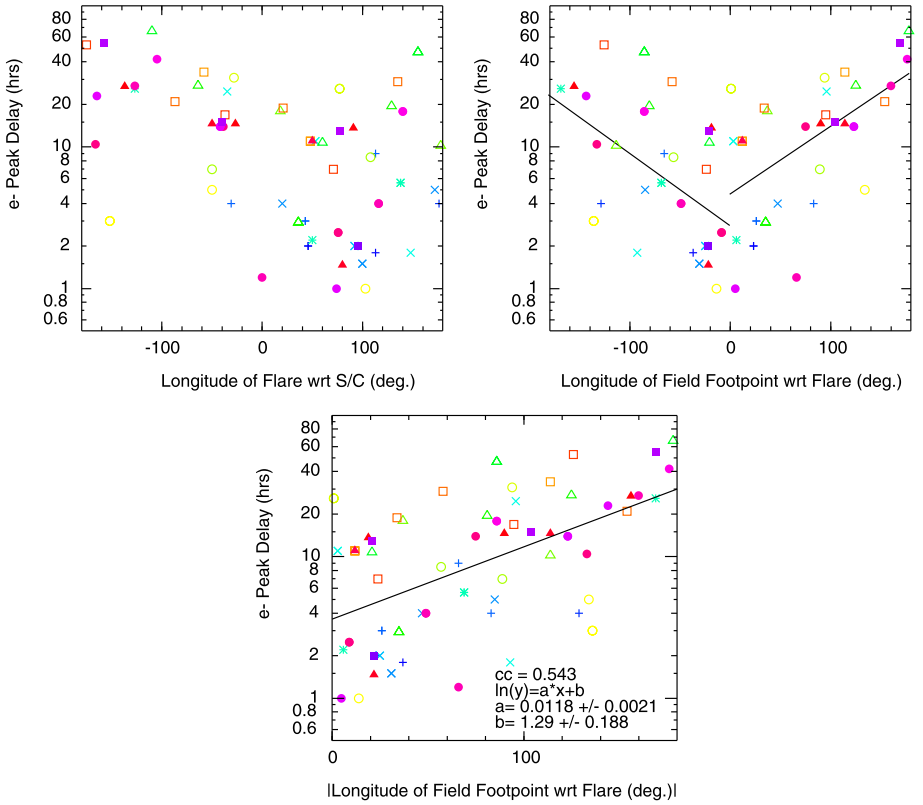

Figure 19 Summary of ∼0.7 – 4 MeV electron peak delays *vs.* flare longitude, connection angle (CA), and |CA|.

from ∼5 for minimal delays to ∼1 – 3 for long delays. Investigating the possible origin of this change in the ratio requires a more complete analysis of the onset times in individual events than is made here. (A possible scenario, for example, is that the initial proton acceleration/injection is delayed relative to electrons.) Nevertheless, the main conclusion to be drawn here is that overall, proton and electron onset delays in three-spacecraft events are highly correlated, both as a function of CA and from event to event. We note that Posner (2007) proposed using observations of near-relativistic electron onsets to give a warning of ∼ one hour or more of the arrival of more hazardous protons and heavier ions with energies of 10s of MeV. The results presented here provide further justification for this technique.

3.3.2. Delays to Peak Intensity

We now consider delays to peak particle intensity. Figure 19 summarizes the delay to peak intensity *versus* event location with respect to the observing spacecraft, CA, and |CA| for ∼0.7 – 4 MeV electrons. As for the onset delays, delays to electron peak intensity are shortest for western-hemisphere/well-connected events. The fits in the top-right panel suggest a slight asymmetry, with shorter delays for cases where the field line connects east of the event, though there is considerable scatter. The fit in the bottom panel indicates a typical delay to electron peak of ∼3.6 hours at zero connection angle, increasing to ∼30 hours at 180° connection angle.

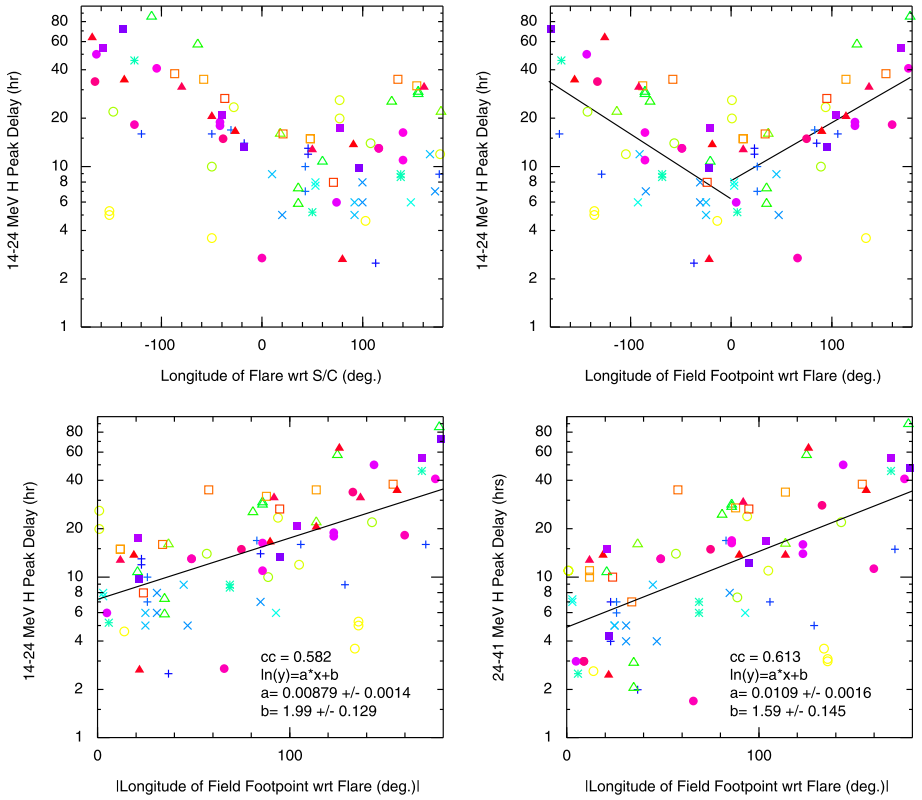

Figure 20 Summary of 14 – 24 MeV proton peak delays *vs.* flare longitude, connection angle (CA), and |CA|. The bottom-right panel shows 24 – 41 MeV proton peak delays *vs.* |CA|.

Figure 20 illustrates similar results for 14 – 24 MeV protons, which again show the shortest delays for western-hemisphere/well-connected events, and approximately symmetrical fits around zero connection angle. Although the focus of our analysis is on the early stages ($\sim$ first day) of SEP events, there are cases, typically for poorly connected events, where particle intensities peak after more extended delays. The fit in the bottom left panel indicates a typical 14 – 24 MeV proton delay to peak at $\sim$ 7.3 hours at zero connection angle, and $\sim$ 40 hours at 180° connection angle. The bottom-right panel shows similar results for 24 – 41 MeV protons; the fit indicates slightly shorter typical delays of $\sim$ 5 hours at zero connection angle, and $\sim$ 30 hours at 180°. The variation of proton peak delay with event longitude is very consistent with that obtained by Van Hollebeke, Ma Sung, and McDonald (1975) for 125 SEP events observed at Earth by IMPs 4 or 5, but by using the STEREO observations, it is possible unambiguously to identify events with far-side sources, and observe events at multiple locations, enabling more events at large connection angles to be included.

Figure 21 shows the correlation between electron and 14 – 24 MeV proton delays to peak intensity. The proton delay is related to the electron delay by $\triangle t_{pH} = 3.7 \triangle t_{pe}^{0.61}$. The right-hand panel shows the ratio of the proton and electron delays as a function of electron delay. The ratio decreases from $\sim$ 4 for the shortest delays, to $\sim$ 1, *i.e.*, similar electron and proton delays to peak intensity, for electron delays above $\sim$ 10 hours.

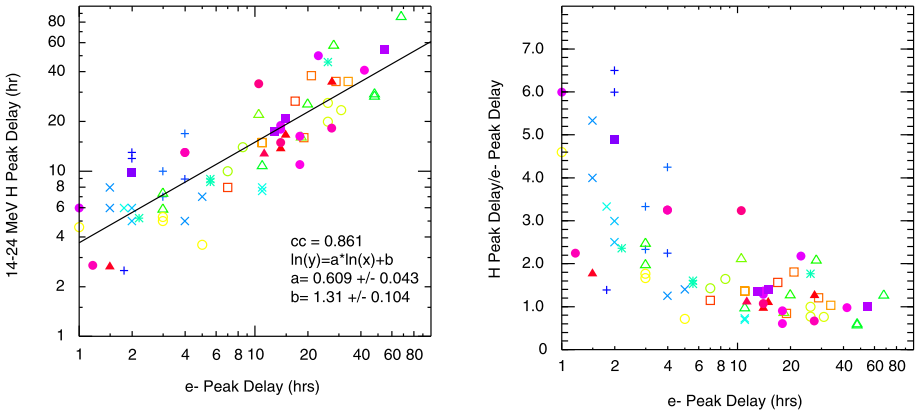

Figure 21 Left: correlation of the electron and proton delays to peak intensity for individual observations of the three-spacecraft events. Right: ratio of proton to electron peak delays as a function of electron onset delay.

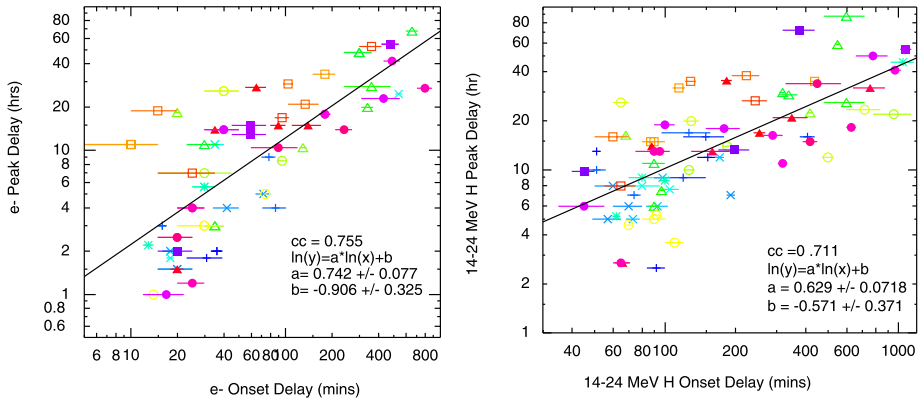

Figure 22 Left: electron peak delay plotted against electron onset delay. Right: 14 – 24 MeV proton peak delays plotted against onset delays.

We finally compare the electron or proton onset and peak delays. Since both increase with connection angle, we might expect some correlation, as is shown to be the case in Figure 22. Although there is an overall correlation, the electron results suggest that for electron onset delays shorter than $\sim$ 1 hour, the delays to peak intensity are highly variable, ranging from $\sim$ 1 to 20 hours. The events to the left of the main distribution have an initial rapid onset followed by a slow rise to peak intensity. It is beyond the scope of this article to investigate the reasons for these differences in the early development of the events, which may involve the evolution of the event at the Sun, interplanetary propagation conditions, and the influence of local structures at the observing spacecraft.

3.3.3. Longitudinal Dependence of SEP Intensity

To investigate the longitudinal dependence of SEP intensity, we again focused on the three-spacecraft events in December 2009 – December 2012. The top row of Figure 23 shows

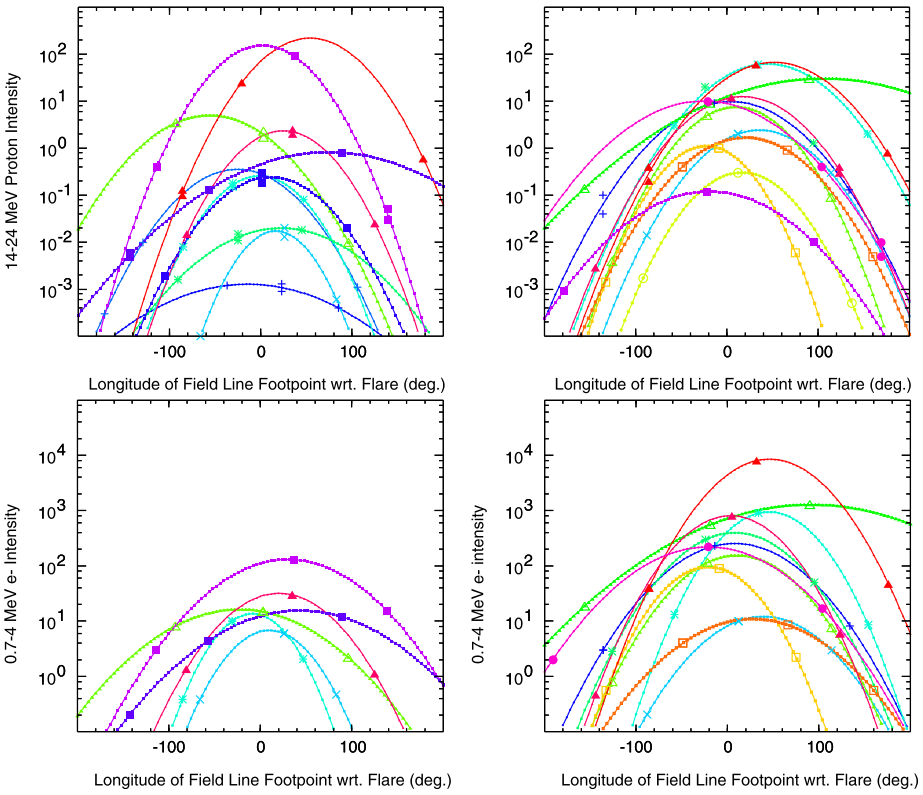

Figure 23 Top row: Gaussian fits to the peak 14 – 24 MeV proton intensity ((MeV s cm^2 sr)$^{-1}$) for three-spacecraft events in (left) December 2009 – October 2011, and (right) November 2011 – October 2012. In some cases, two estimates of the intensity at SOHO (from ERNE and EPHIN) are shown. A background of 10^{-4} (MeV s cm^2 sr)$^{-1}$ has been removed. Bottom row: Gaussian fits to the peak $\sim$0.3 – 4 MeV electron intensity ((MeV s cm^2 sr)$^{-1}$) for three-spacecraft events in (left) December 2009 – October 2011, and (right) November 2011 – October 2012. STEREO HET intensities have been multiplied by the factors discussed in Section 2.

Gaussian fits $I(\phi) = I_o e^{-(\phi-\phi_o)^2/2\sigma^2}$ to background-corrected 14 – 24 MeV proton intensities plotted *versus* connection angle (ϕ), for the events where such a fit can be made. The left and right panels show events up to or after October 2011, respectively, to reduce the number of superposed graphs. The peak intensities (I_o) of the Gaussian fits cover $\sim$5 orders of magnitude, again illustrating that the three-spacecraft events cover a wide range of intensities. However, the weaker events, with $I_o < 10^{-1}$ (MeV s cm^2 sr)$^{-1}$, evidently were predominantly observed before October 2011.

The top left panel of Figure 24 shows that the connection angles of the peaks of the Gaussian fits (ϕ_o) tend to cluster around the longitude of the solar event. The average offset is 15.1° west, *i.e.*, peak intensities, on average, are found on field lines that connect $\sim$15° west of the solar event. However, the distribution is broad, with a standard deviation of 35.2°, so the results do not appear to indicate any consistent west/east bias. Uncertainty in the location of the solar event, which may be extended and not accurately represented by the location of the related flare or other feature, and errors in inferring the spacecraft magnetic connection to the Sun, probably also contribute to the offset. The top-right panel

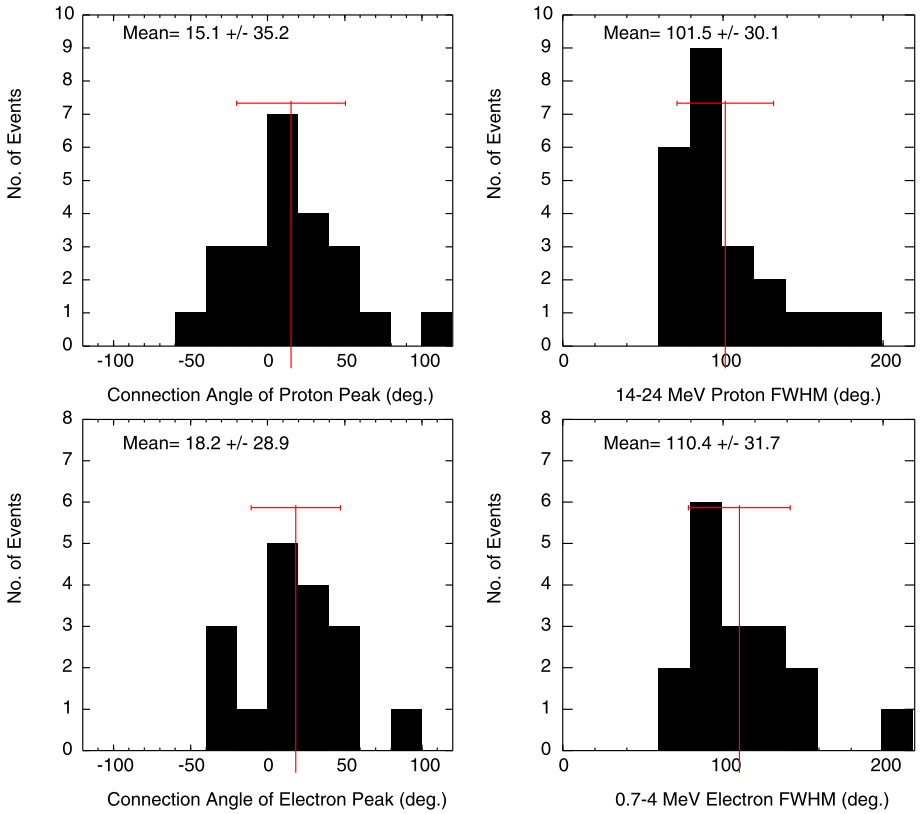

Figure 24 Distributions of the connection angle of the maximum intensity and the full width at half maximum for proton (top row) and electron (bottom row) Gaussian fits to the three-spacecraft events in Figure 23.

of Figure 24 shows the distribution of full widths at half maximum (FWHM, $\approx 2.355\sigma$) for 14 – 24 MeV protons. The average FWHM is 101.5° with a standard deviation of 30.1°, corresponding to $\sigma = 43 \pm 13°$. This is similar to $\sigma = 45 \pm 2°$ ($\sigma = 43 \pm 2°$) found by Lario *et al.* (2013) for an independent (though overlapping) sample of 25 – 53 MeV (15 – 40 MeV) proton events in 2009 – 2012, and the $\sigma = 36 \pm 2°$ obtained by Lario *et al.* (2006) for 27 – 37 MeV proton events in Solar Cycle 21. Longitudinal SEP intensity dependencies inferred from multispacecraft observations were also reported by Kallenrode (1993), though Gaussian fits were not made.

The bottom panels in Figures 23 and 24 show similar results for $\sim 0.7 - 4$ MeV electrons for the events where such a fit can be made. The same symbols are used for each event in the proton and electron plots. For protons, the average footpoint location of the electron Gaussian maxima is displaced slightly to the west of the solar event by a similar angle (18.2°), though with a standard deviation of 28.9°. The electron FWHM is also similar to that for protons ($110 \pm 32°$), corresponding to $\sigma = 47 \pm 14°$. This value is consistent with the $\sigma = 49 \pm 2°$ ($\sigma = 46 \pm 2°$) obtained by Lario *et al.* (2013) for 71 – 112 keV (0.7 – 3 MeV) electrons. The comparable σs for electrons and protons imply that intensities decline with increasing longitude from the solar event at similar rates. We also note that Wiedenbeck *et al.* (2013) examined a ^{3}He-rich impulsive event on 7 February 2010 (unrelated to the 25 MeV

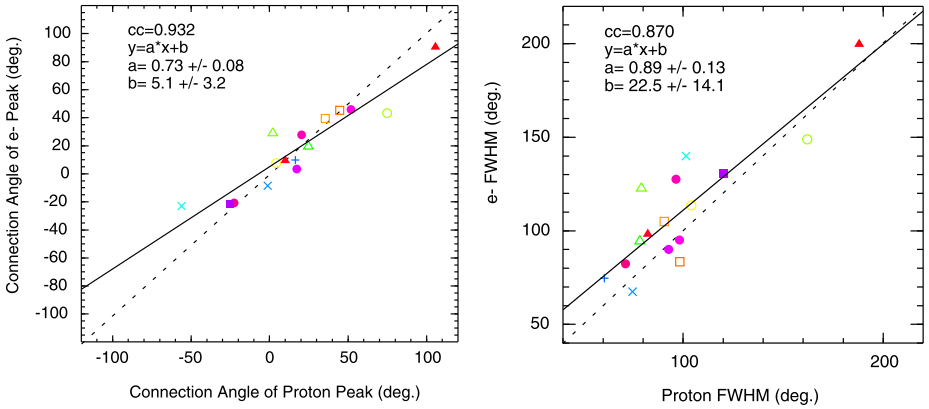

Figure 25 Correlation of proton and electron Gaussian peak connection angles (left) and FWHM (right) for three-spacecraft events. Symbols indicate events. The dashed lines indicate equal values for protons and electrons.

proton event on this day in Table 1) that was observed at the two STEREO spacecraft and by ACE when separated by 136° in longitude, and found that the ∼3 MeV n^{-1} ^{3}He fluence (event-integrated intensity) decreased with longitude with $\sigma = 48°$. These similar values of σ may suggest a common propagation scenario for ^{3}He in impulsive events and protons and electrons in the early stages of gradual SEP events. We also note that Kallenrode (1993) concluded that longitudinal intensity dependencies are similar for "impulsive" events, defined in that study by the X-ray flare duration (*cf.*, Cane, McGuire, and von Rosenvinge, 1986), and other events.

The left-hand panel of Figure 25 shows that proton and electron Gaussian peaks in individual events tend to occur at similar connection angles – the dashed line indicates equality – while the best fit suggests a trend for the electron peak to be slightly closer to the event location. The proton and electron FWHMs are also correlated (right-hand panel of Figure 25), though the electron widths generally slightly exceed the proton widths, typically by ∼10°.

Figure 26 shows, for 14 – 24 MeV protons (top row) and 0.7 – 4 MeV protons (bottom row), the intensity of the peak of the Gaussian fit (left-hand panels) or FWHM (right-hand panels) plotted against the LASCO CME speed. As for the observed proton intensities of western-hemisphere events in Figure 14, the proton Gaussian heights are correlated with the CME speed. The scatter in the points is reduced, as might be expected because variations due to connection angle are no longer present. The electron peak intensity shows a weaker trend with CME speed. The CME speed shows no (for protons) or little (for electrons) correlation with the FWHM. Thus, the observations do not appear to favor a scenario in which a faster CME results in a wider particle event that decreases less rapidly with longitude.

3.4. A Typical Event

The above observations suggest the following characteristics of a typical three-spacecraft SEP event: from the time of type III emission onset, ∼0.7 – 4 MeV electrons arrive at a spacecraft *directly connected to the event* typically in ∼19 minutes, while 14 – 24 MeV protons do so after ∼54 minutes. The additional proton delay may be largely accounted for by the difference in the particle speeds along a nominal magnetic field line. For a spacecraft on a field line with a connection angle $\phi(°)$ east or west of the solar event, particle arrival

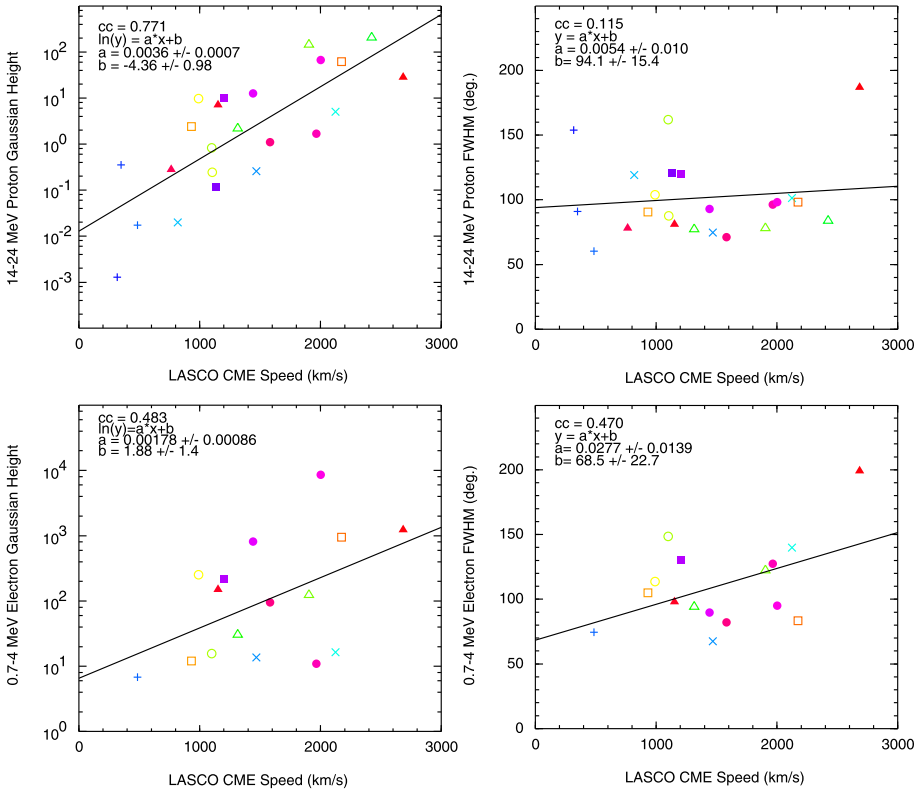

Figure 26 Correlation of LASCO CME speeds with proton (top row) and electron (bottom row) Gaussian peak heights and FWHMs for three-spacecraft events. Symbols indicate events.

relative to the type III burst is delayed by $\triangle t_{oe} \approx 19\exp(0.0153\phi)$ minutes for 0.7 – 4 MeV electrons (Figure 15) or $\triangle t_{oH} \approx 54\exp(0.0154\phi)$ minutes for 14 – 24 MeV protons (Figure 16). The peak intensity is delayed by $\triangle t_{pe} \approx 3.6\exp(0.0118\phi)$ hours for 0.7 – 4 MeV electrons and $\triangle t_{pH} \approx 7.3\exp(0.0088\phi)$ hours for 14 – 24 MeV protons. The peak intensity (not associated with passage of an interplanetary shock) decreases with connection angle with FWHMs of $\sim 100°$ ($\sigma \approx 43°$) for protons and $\sim 110°$ ($\sigma \approx 47°$) for electrons based on Gaussian fits. The peaks of the 14 – 24 MeV Gaussian fits are correlated with the CME speed V (km s^{-1}) as $I_o \approx 0.013\exp(0.0036V)$ (MeV s cm^2 sr)$^{-1}$. (The observed particle intensity is also correlated with the soft X-ray flare intensity (Figure 14), but there are too few events with Gaussian fits and associated X-ray observations to infer a similar correlation. Combining these results, the typical peak 14 – 24 MeV proton intensity (early in the event) at a spacecraft at 1 AU with a connection angle ϕ associated with a CME of speed V is given by $I(\phi)$ (MeV s cm^2 sr)$^{-1} \approx 0.013\exp(0.0036V - \phi^2/2\sigma^2))$, $\sigma = 43°$. Figure 27 shows the predicted 14 – 24 MeV proton intensity based on this formula for 544 SEP events observed at Earth during 1996 – 2013 (including events from Cane, Richardson, and von Rosenvinge, 2010a), or at STEREO A or B, plotted against the observed peak 25 MeV proton intensity for these events. For simplicity, we assumed for all events that the solar wind speed is 450 km s^{-1} when we calculated the connection angle, and that peak SEP intensity at the Sun occurs at the longitude of the solar event. The predicted and observed intensities show a fair

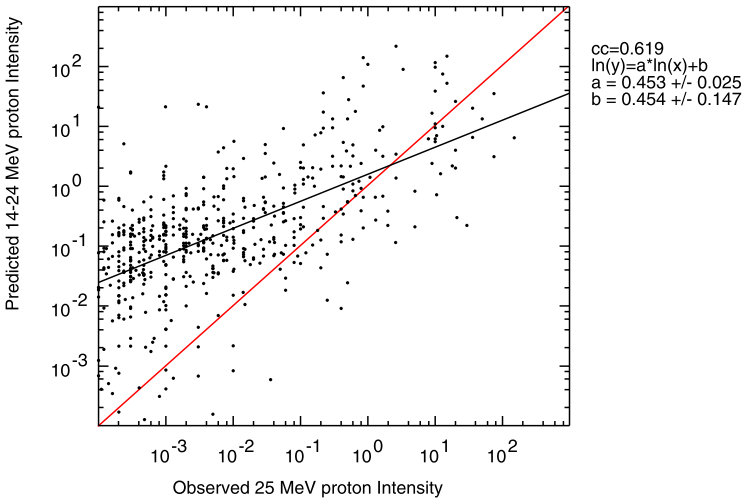

Figure 27 Predicted 14 – 24 MeV proton intensity based on the relationship between intensity and CME speed, and longitudinal dependence for three-spacecraft events, plotted against the observed intensity at 25 MeV for 532 SEP events observed at Earth and/or at STEREO A/B in 1996 – 2013. The red line indicates equality.

correlation (cc = 0.619), but there is considerable scatter, of around an order of magnitude above and below the fitted (black) line. Furthermore, the predicted intensities for the weaker events tend to be overestimated – the red line indicates equality. This is also illustrated in Figure 28, which shows the predicted 14 – 24 MeV and observed ∼25 MeV proton intensities for the 544 SEP events as a function of event longitude (left) and connection angle (right). The intensity variation with longitude/connection angle for the largest events is reasonably well predicted, as might be expected since the formula was developed using such events, suggesting that it may have a potential for forecasting the intensities of the largest events that are of particular interest for space weather. Nevertheless, it is clear that the formula, based only on CME speed and CA, overestimates the intensity for a large population of events. This is also evident from comparing the proton intensity–CME speed relationship for western-hemisphere events in Figure 14 and for the three-spacecraft event Gaussian peaks in Figure 26, noting the ∼2 orders of magnitude difference in the intensities for events associated with slower CMEs. Comparison of Figures 28 and 12 suggests that many of these weaker events have characteristics similar to the one- and two-spacecraft events discussed above. However, many of the SEP events in Figure 28 are from the pre-STEREO era, so the actual longitudinal extent of these events cannot be determined.

3.5. Implications for Particle Transport near the Sun and in the Solar Wind

We now very briefly discuss the implications of the above observations for particle transport in longitude near the Sun and/or in the solar wind. There are a number of processes that might be involved including:

- *Multiple particle injections from sympathetic flares:* for the three-spacecraft events we examined, we find no clear case in which multiple solar events in different active regions that occur close in time played a role in producing what appears to be a single, longitudinally extended particle event.

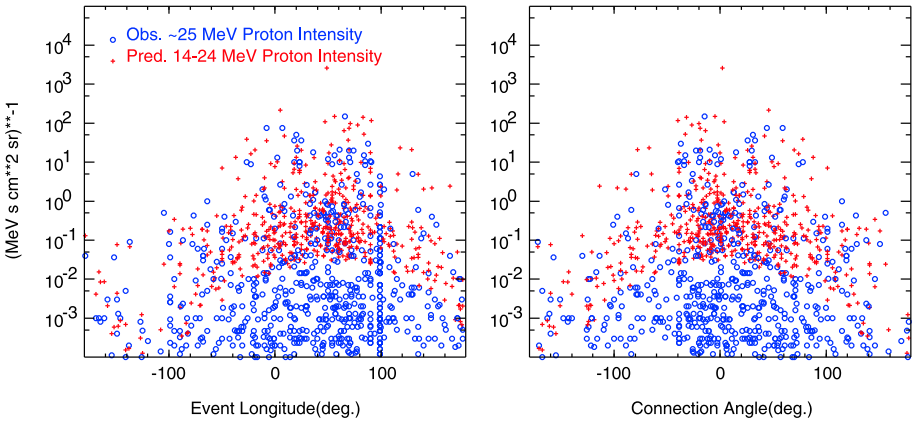

Figure 28 Predicted 14 – 24 MeV proton intensity (red crosses) and observed ∼25 MeV proton intensity (blue circles) plotted against the solar event longitude relative to the observing spacecraft (left) and connection angle (right) for 544 SEP events observed at Earth and/or at STEREO A/B in 1996 – 2013.

- *Cross-field transport/diffusion in the solar wind:* cross-field particle transport in the solar wind is generally expected to be a slower process than parallel transport, as indicated for example by the clear influence of the spiral interplanetary magnetic field on particle transport we found, and by the particle intensity drop-outs observed in some events by Mazur *et al.* (2000). Giacalone and Kóta (2012) have modeled the transport of particles in the solar wind from an impulsive event, motivated by the observations of Wiedenbeck *et al.* (2013). In addition to cross-field diffusion, an important effect is the corotation of the IMF, which moves the particle population toward the west, so that the particles can be detected, with some delay, at spacecraft lying some distance west of the event. While this type of process may contribute to the observation of particles from far-eastern events, cross-field transport in the solar wind is probably is too slow to account for the typical onset delays at CA = 180° of ∼5 hours for electrons and ∼14 hours for protons suggested by our analysis. The prompt onset at widely separated spacecraft on 3 November 2011 (Figure 7) provides a particular challenge for a scenario of longitudinal particle transport in the solar wind. On the other hand, we note that Dresing *et al.* (2012) favored a role for strong perpendicular diffusion in the 17 January 2010 SEP event based on the results of a 3D particle transport model. A similar process has been also modeled recently by Marsh *et al.* (2013) and Lampa and Kallenrode (2009), who concluded that it may contribute significantly to SEP longitudinal transport.
- *Diffusion near/at the Sun/coronal propagation:* this process has been widely studied in the past as a method of distributing solar particles in longitude (*e.g.*, Reinard and Wibberenz, 1974; Newkirk and Wentzel, 1978; Perez-Peraza, 1986), in particular before it was recognized that particle acceleration at extended CME-driven shocks could fulfill this role in large SEP events (*e.g.*, Cane, Reames, and von Rosenvinge, 1988). It was also suggested by Wibberenz and Cane (2006) to be occurring during impulsive electron events. The tendency for east–west symmetry in the onset and peak delays and the close correlation of the electron and proton delays might be suggestive of some type of diffusive process near to the Sun, at least early in gradual events.
- *Acceleration by expansive interplanetary or coronal shocks:* Cliver *et al.* (1995) noted that SEP events can turn on rapidly even at large connection angles (for example, within

two hours for $\sim$1 MeV electrons for connection angles up to $\sim$150°; *cf.* the similar results in Figure 15). Considering such events in the context of shock acceleration, they concluded that acceleration at CME-driven shocks in the solar wind cannot be responsible for these rapid distant onsets since such shocks appear to be limited to longitudinal extents of $\sim$180°. As an alternative, acceleration by essentially circum-solar coronal shocks, with propagation speeds of $\sim 200-500$ km s^{-1} (based on electron onset delays) was proposed. Cliver *et al.* (1995) did not examine proton onset delays in detail, but suggested that differences in the proton and electron onset delays, as inferred in the present study, might pose a problem for this scenario (as also noted by Kallenrode (1993) for coronal shocks in general), as might events with longer delays.

- *Connection to an expanding three-dimensional CME shock:* STEREO and SOHO observations now allow the three-dimensional structure of CMEs and their associated shocks to be inferred close to the Sun. Assuming that SEPs are accelerated by CME-driven shocks, a reasonable scenario is that SEPs are injected onto interplanetary field lines when the expanding shock intersects these field lines. For example, Rouillard *et al.* (2012) concluded that the interspacecraft particle onset delays in the 21 March 2011 event (Figure 5) were consistent with connection to an expanding CME shock observed by STEREO and SOHO. We have identified additional extended SEP events that may be used to establish whether this is a general result.
- *Association with EUV waves:* since the discovery of EUV waves by the EIT instrument on SOHO, the possibility that particles are injected as such an expanding EUV wave intercepts the footpoints of magnetic-field lines has been considered (*e.g.*, Bothmer *et al.*, 1997; Krucker *et al.*, 1999). Rouillard *et al.* (2012) noted that an EUV wave tracked the laterally expanding flank of the 21 March 2011 CME, moving parallel to the surface of the Sun at $\sim$450 km s^{-1}. AIA observations of EUV waves suggest that initial speeds may reach $600-2000$ km s^{-1}, but such waves decelerate rapidly, and typical final speeds are $180-380$ km s^{-1} (Patsourakos and Vourlidas, 2012, and references therein). Such speeds are fairly similar to the typical source speeds inferred in Figures 15, 16, and 17, in particular for protons, suggesting that EUV waves might be linked to the spread of SEPs in longitude. Nitta *et al.* (2013) have recently reported higher speeds (mean = 644 km s^{-1}; median = 607 km s^{-1}) for large-scale coronal propagating fronts observed by AIA and noted that these speeds were weakly correlated with the expansion speeds of the associated CMEs, which may be consistent with the lack of correlation between source and CME speeds in Figure 17. As for the coronal-shock scenario above, the different electron and proton onset delays and inferred source speeds may pose a problem. In addition, an exceptionally fast and widespread EUV wave, extending to the footpoints of field lines connecting to STEREO B and Earth might have been expected to be associated with the 3 November 2011 event (Figure 6), but it appears that AIA did not observe such a wave (N. Nitta, private communication, 2012; Nitta *et al.*, 2013). Of the 171 fronts reported by Nitta *et al.* (2013), 55 (32 %) were associated with SEP events identified in this study, while of the 94 SEP events originating at E120° to W120°, the approximate range of the sources of the fronts reported by Nitta *et al.* (2013), 53 (56 %) were associated with such a front. Of these 53 events, 14 (26 %) were single-spacecraft, 20 (38 %) were two-spacecraft, and 12 (23 %) were three-spacecraft events (for the remaining events, the number of spacecraft is uncertain), suggesting that observation of a propagating front is not strongly related to the observed extent of the SEP event.
- *Particle transport to remote longitudes by large-scale magnetic loops:* reconstructions of coronal magnetic fields based on photospheric magnetic-field observations (*e.g.*, Schrijver *et al.*, 2013) suggest the existence of large-scale magnetic loops that might guide SEPs

to locations far from the original solar event. Furthermore, modeling of the evolution of coronal magnetic fields during a CME (Masson, Antiochos, and DeVore, 2013) indicates that reconnection between closed and open field lines may lead to field configurations that facilitate particle transport to locations far removed from the original solar event. However, it is unclear whether the tendency for east–west symmetry in event delays and intensities and their ordering by connection angle, at least taken over the ensemble of events, would be consistent with this scenario, although it might play a role in particular events.

- *Guidance by nonspiral interplanetary magnetic fields:* Richardson, Cane, and von Rosenvinge (1991) discussed cases where SEPs arrived promptly from weakly connected solar events by being guided within interplanetary coronal mass ejections that happened to be passing the observing spacecraft at the times of the events. We examined the solar wind present at the three spacecraft at the times of the three-spacecraft SEP events, and in general found no evidence of such structures, although there are exceptions where local solar-wind structure does appear to influence the development of SEP events at a particular spacecraft, leading to some of the outliers in the distributions discussed above. However, a discussion of such events is beyond the scope of this article.

4. Summary

We have used observations of protons and electrons from the HETs on the STEREO A and B spacecraft and from the ERNE and EPHIN instruments on SOHO to summarize the properties of solar particle events that included $\sim$25 MeV protons since the beginning of the STEREO mission in October 2006 until December 2013. The major conclusions are the following:

- Some 209 unique >25 MeV proton events were detected during the study period by the STEREO spacecraft and/or at Earth. All of the events, at least up to the end of the CDAW LASCO catalog at the time of writing (May 2013), were accompanied by CMEs.
- Considering events between December 2009 and December 2012, when the spacecraft were well separated, 36 % were detected by only one spacecraft, 34 % by only two, and 17 % by all three spacecraft, depending on factors such as whether particular spacecraft are well or poorly connected to the solar event by the nominal Parker spiral IMF, and the intensity of the event. Around 30 % of the events were not detected at Earth.
- While the most intense events at well-connected spacecraft, and those associated with the fastest CMEs, tend to be three-spacecraft events, the intensity observed at the best-connected spacecraft, or the CME speed, for example, are not reliable predictors of the visibility at the other spacecraft.
- 92 % of the SEP events were accompanied by type III radio emissions observed by the WIND/WAVES or STEREO/SWAVES instruments, while 53 % had type II emissions, and 33 % IP type II emissions extending below 1 MHz.
- The percentage of events associated with type II emissions increases with the number of spacecraft that detected the event, reaching 81 % for three-spacecraft events, including $\sim$60 % with IP type II emissions.
- Single-spacecraft events typically occur at well-connected longitudes, have peak intensities at $\sim$25 MeV of $< 10^{-2}$ (MeV s cm^2 sr)$^{-1}$, and are accompanied by CMEs with speeds below 1000 km s^{-1}. Type II emissions are reported in only 25 % of cases.

- The availability of STEREO observations of the far side of the Sun confirms the results of previous studies using only observations at Earth that around a quarter of >25 MeV proton events originate behind the west limb with respect to the observer, and occasionally ($\sim 4-8$ % of events) behind the east limb. Energetic particles are unambiguously observed from solar activity $\sim 180°$ in longitude from the observation point and on field lines that have footpoints at the Sun $\sim 180°$ from the solar event.
- SEP occurrence rates at Earth were fairly similar during the rising phases of Cycles 23 and 24. However, the first event was detected at Earth one year after smoothed sunspot minimum in Cycle 24 compared with a delay of only two months in Cycle 23. The first two years of Cycle 24 were characterized by brief intervals with SEP activity followed by low-activity intervals of $\sim$ six months that may be evidence of a quasi-periodicity similar to that described by Rieger *et al.* (1984).
- The SEP rate during 2013 declined from that in 2011 and 2012, but shows evidence of an increase in the final months of 2013 that appears to be associated with an increase in the number of southern-hemisphere sunspots. The lower SEP rate in $2012-2013$ relative to 2011 may be a manifestation of the Gnevyshev gap in energetic solar activity that is often observed during solar cycle maxima.
- Longitudinal dependencies of the electron and proton peak intensities and delays to onset and peak were examined for three-spacecraft events. Both delays to onset and delays to peak increase with increasing connection angle between the solar event and the footpoint of magnetic-field lines passing the observing spacecraft. The results suggest a close coupling between energetic protons and electrons such as correlated onset and peak delays and similar intensity dependence with longitude.
- The 3 November 2011 event had an exceptionally rapid turn-on at all three spacecraft, with a difference in the ~ 25 MeV proton onset times of only ~ 25 minutes. The CME speed, however, was quite normal (991 km s^{-1}).
- A formula predicting the proton intensity at $14-24$ MeV based on the CME speed and solar event location was developed using three-spacecraft event observations. While it appears to predict the intensity of the largest, most extended events reasonably well, it fails for a large population of weaker-than-expected events.
- The tendency for east–west symmetry in the delays to onset and peak, and the Gaussian fits to peak around zero connection longitude suggest that electron and proton propagation in longitude away from the solar event occurs somewhat symmetrically. This may be most consistent with a scenario involving a propagating shock or wave moving out from the event, although different source propagation speeds inferred for electrons and protons may be a complication, or some sort of diffusive process.

Acknowledgements We thank Janet Luhmann of the University of California, Berkeley, for her steadfast support as the Principal Investigator of the STEREO/IMPACT investigation. The work at GSFC, Caltech and JPL was supported by NASA (Caltech and JPL were funded under subcontract SA2715-26309 from the University of California, Berkeley, under NASA Contract NAS5-03131). The LASCO CME catalog at http://cdaw.gsfc.nasa.gov/CME_list/ is generated and maintained at the CDAW Data Center by NASA and The Catholic University of America in cooperation with the Naval Research Laboratory. We particularly appreciate the efforts by S. Yashiro and colleagues to generate daily summary movies of SOHO and STEREO observations (http://cdaw.gsfc.nasa.gov/stereo/daily_movies/), which were very helpful in verifying the solar sources of the SEP events. The CACTUS CME catalog is maintained by the Solar Influences Data Analysis Center at the Royal Observatory of Belgium. The SOHO/ERNE data were obtained from the Space Research Laboratory, University of Turku (http://www.srl.utu.fi/erne_data/). The SOHO/EPHIN project is supported under grant No. 50 OC 1302 by the German Bundesminister für Wirtschaft through the Deutsches Zentrum für Luft- und Raumfahrt (DLR). SOHO is a project of international cooperation between ESA and NASA.

References

Bazilevskaya, G.A., Makhmutova, V.S., Sladkova, A.I.: 2006, *Adv. Space Res.* **38**(3), 484.

Bothmer, V., Posner, A., Kunow, H., Müller-Mellin, R., Heber, B., Pick, M., *et al.*: 1997, In: *Proc. 31st ESLAB Symp. "Correlated Phenomena at the Sun in the Heliosphere, and in Geospace* **SP-415**, ESA, Noordwijk, 207.

Brueckner, G.E., Howard, R.A., Koomen, M.J., Korendyke, C.M., Michels, D.J., Moses, J.D., *et al.*: 1995, *Solar Phys.* **162**, 357.

Cane, H.V.: 1985, *J. Geophys. Res.* **90**, 191.

Cane, H.V., Erickson, W.C., Prestage, N.P.: 2002, *J. Geophys. Res.* **107**(A10), 1315. DOI.

Cane, H.V., Erickson, W.C.: 2003, *J. Geophys. Res.* **108**(A5), 1203. DOI.

Cane, H.V., Erickson, W.C.: 2005, *Astrophys. J.* **623**, 1180.

Cane, H.V., Kahler, S.W., Sheeley, N.R., Jr.: 1986, *J. Geophys. Res.* **91**, 13321.

Cane, H.V., McGuire, R.E., von Rosenvinge, T.T.: 1986, *Astrophys. J.* **301**, 448.

Cane, H.V., Reames, D.V., von Rosenvinge, T.T.: 1988, *J. Geophys. Res.* **93**, 9555.

Cane, H.V., Richardson, I.G., von Rosenvinge, T.T.: 1998, *Geophys. Res. Lett.* **25**, 4437.

Cane, H.V., Richardson, I.G., von Rosenvinge, T.T.: 2010a, *J. Geophys. Res.* **115**, A08101. DOI.

Cane, H.V., Richardson, I.G., von Rosenvinge, T.T.: 2010b. In: Maksimovic, M. *et al.* (eds.) *Twelfth International Solar Wind Conference*, *AIP Conf. Proc.* **1216**, 687.

Cane, H.V., Stone, R.G.: 1984, *Astrophys. J.* **282**, 339.

Cane, H.V., Stone, R.G., Fainberg, J., Steinberg, J.L., Hoang, S.: 1982, *Solar Phys.* **78**, 187.

Chowdhury, P., Choudhary, D.P., Gosain, S.: 2013, *Astrophys. J.* **768**, 188. DOI.

Cliver, E.W., Kallenrode, M.-B.: 2001. In: *Proc. 27th Int. Cosmic Ray Conf.* **8**, 3318.

Cliver, E.W., Kahler, S.W., Neidig, D.F., Cane, H.V., Richardson, I.G., Kallenrode, M.-B., Wibberenz, G.: 1995. In: *Proc. 24th Int. Cosmic Ray Conf.* **4** 257.

Dalla, S., Balogh, A., Heber, B., Lopate, C.: 2001, *J. Geophys. Res.* **106**, 5721.

Delaboudinière, J.-P., Artzner, G.E., Brunaud, J., Gabriel, A.H., Hochedez, J.F., Millier, F.: 1995, *Solar Phys.* **162**, 291.

Dresing, N., Gómez-Herrero, R., Klassen, A., Heber, B., Kartavykh, Y., Dröge, W.: 2012, *Solar Phys.* **281**, 281. DOI.

Feminella, F., Storini, M.: 1997, *Astron. Astrophys.* **322**, 311.

Giacalone, J., Kóta, J.: 2012, *Astrophys. J.* **751**, L33.

Gnevyshev, M.N.: 1967, *Solar Phys.* **1**, 107.

Gnevyshev, M.N.: 1977, *Solar Phys.* **51**, 175.

Gopalswamy, N., Yashiro, S., Michalek, G., Kaiser, M.L., Howard, R.A., Reames, D.V., *et al.*: 2002, *Astrophys. J. Lett.* **572**, L103.

Gopalswamy, N., Yashiro, S., Krucker, S., Stenborg, G., Howard, R.A.: 2004, *J. Geophys. Res.* **109**, A12. DOI.

Howard, R., Moses, J.D., Vourlidas, A., Newmark, J.S., Socker, D.G., Plunkett, S.P., *et al.*: 2008, *Space Sci. Rev.* **136**, 67.

Kahler, S.W.: 2001, *J. Geophys. Res.* **110**, A12S01.

Kahler, S.W., Hildner, E., Van Hollebeke, M.A.I.: 1978, *Solar Phys.* **57**, 429.

Kahler, S.W., Sheeley, N.R. Jr., Howard, R.A., Michels, D.J., Koomen, M.J., McGuire, R.E., *et al.*: 1984, *J. Geophys. Res.* **89**, 9683. DOI.

Kallenrode, M.-B.: 1993, *J. Geophys. Res.* **98**, 5573.

Krucker, S., Larson, D.E., Lin, R.P., Thompson, B.J.: 1999, *Astrophys. J.* **519**, 864.

Lampa, F., Kallenrode, M.-B.: 2009, *Solar Phys.* **260**, 423. DOI.

Lario, D., Kallenrode, M.-B., Decker, R.B., Roelof, E.C., Krimigis, S.M., Aran, A., Sanahuja, B.: 2006, *Astrophys. J.* **653**, 1531.

Lario, D., Aran, A., Gómez-Herrero, R., Dresing, N., Heber, B., Ho, G.C., Decker, R.B., Roelof, E.C.: 2013, *Astrophys. J.* **767**, 41.

Lean, J.L.: 1990, *Astrophys. J.* **363**, 718.

Lemen, J.R., Title, A.M., Akin, D.J., Boerner, P.F., Chou, C., Drake, J.F., *et al.*: 2012, *Solar Phys.* **275**, 17. DOI.

Leske, R.A., Cohen, C.M.S., Dotson, B., Mewaldt, R.A., Cummings, A.C., Labrador, A.W., *et al.*: 2013. In: *Thirteenth International Solar Wind Conference*, *AIP Conf. Proc.* **1539**, 227. DOI.

Levy, E.H., Duggal, S.P., Pomerantz, M.A.: 1976, *J. Geophys. Res.* **81**, 51.

Li, G., Moore, R., Mewaldt, R.A., Zhao, L., Labrador, A.W.: 2012, *Space Sci. Rev.* **171**, 141. DOI.

Marsh, M.S., Dalla, S., Kelly, J., Laitinen, T.: 2013, *Astrophys. J.* **774**, 4. DOI.

Masson, S., Antiochos, S.K., DeVore, C.R.: 2013, *Astrophys. J.* **771**, 82.

Mazur, J.E., Mason, G.M., Dwyer, J.R., Giacalone, J., Jokipii, J.R., Stone, E.C.: 2000, *Astrophys. J.* **532**, L79.
Moon, Y.-J., Choe, G.S., Park, Y.D., Wang, H., Gallagher, P.T., Chae, J., Yun, H.S., Goode, P.R.: 2002, *Astrophys. J.* **574**, 434.
Müller-Mellin, R., Kunow, H., Fleissner, V., Pehlke, E., Rode, E., Röschmann, N., *et al.*: 1995, *Solar Phys.* **162**, 483.
Newkirk, G. Jr., Wentzel, D.G.: 1978, *J. Geophys. Res.* **83**, 2009.
Nitta, N.V., Schrijver, C.J., Title, A.M., Liu, W.: 2013, *Astrophys. J.* **776**, 58. DOI.
Nolte, J.T., Roeloff, E.C.: 1973, *Solar Phys.* **33**, 241.
Norton, A.A., Gallagher, J.G.: 2010, *Solar Phys.* **261**, 193.
Patsourakos, S., Vourlidas, A.: 2012, *Solar Phys.* **281**, 187.
Perez-Peraza, J.: 1986, *Space Sci. Rev.* **44**, 91.
Pomerantz, M.A., Duggal, S.P.: 1974, *J. Geophys. Res.* **79**, 913.
Posner, A.: 2007, *Space Weather* **5**, S05001. DOI.
Reinard, R., Wibberenz, G.: 1974, *Solar Phys.* **36**, 473.
Richardson, R.S.: 1936, *Annu. Rep. Dir. Mt. Wilson Obs.* **35**, 871.
Richardson, I.G., Cane, H.V., von Rosenvinge, T.T.: 1991, *J. Geophys. Res.* **96**, 7853.
Richardson, I.G., Cane, H.V.: 2005, *Geophys. Res. Lett.* **32**, L02104.
Richardson, I.G., Cane, H.V.: 2010, *Solar Phys.* **264**, 189.
Richardson, I.G., Cane, H.V.: 2012, *J. Space Weather Space Clim.* **2**, A02.
Rieger, E., Share, G.H., Forrest, D.J., Kanbach, G., Reppin, C., Chupp, E.L.: 1984, *Nature* **312**, 623.
Rouillard, A.P., Sheeley, N.R. Jr., Tylka, A., Vourlidas, A., Ng, C.K., Rakowski, C., *et al.*: 2012, *Astrophys. J.* **752**, 44.
Schrijver, C.J., Title, A.M.: 2011, *J. Geophys. Res.* **116**, A04108. DOI.
Schrijver, C.J., Title, A.M., Yeates, A.R., DeRosa, M.L.: 2013, *Astrophys. J.* **773**, 93.
Storini, M., Bazilevskaya, G.A., Flückiger, E.O., Krainev, M.B., Makhmutov, V.S., Sladkova, A.I.: 2003, *Adv. Space Res.* **31**(4), 895.
Torsti, J., Valtonen, E., Lumme, M., Peltonen, P., Eronen, T., Louhola, M., *et al.*: 1995, *Solar Phys.* **162**, 505.
Vainio, R., Valtonen, E., Heber, B., Malandraki, O.E., Papaioannou, A., Klein, K.-L., *et al.*: 2013, *J. Space Weather Space Clim.* **3**, A12.
Van Hollebeke, M.A.I., Ma Sung, L.S., McDonald, F.B.: 1975, *Solar Phys.* **41**, 189.
von Rosenvinge, T.T., Reames, D.V., Baker, R., Hawk, J., Nolan, J.T., Ryan, L., *et al.*: 2008, *Space Sci. Rev.* **136**, 391. DOI.
von Rosenvinge, T.T., Richardson, I.G., Reames, D.V., Cohen, C.M.S., Cummings, A.C., Leske, R.A., *et al.*: 2009, *Solar Phys.* **256**, 443.
Wibberenz, G., Cane, H.V.: 2006, *Astrophys. J.* **650**, 1199.
Wiedenbeck, M.E., Mason, G.M., Cohen, C.M.S., Nitta, N.V., Gómez-Herrero, R., Haggerty, D.K.: 2013, *Astrophys. J.* **762**, 54.
Wülser, J.-P., Lemen, J.R., Tarbell, T.D., Wolfson, C.J., Cannon, J.C., Carpenter, B.A., Duncan, D.W., *et al.*: 2004, In: *Telescopes and Instrumentation for Solar Astrophysics*, *Proc. SPIE* **5171**, 111. DOI.
Yashiro, S., Gopalswamy, N., Michalek, G., St. Cyr, O.C., Plunkett, S.P., Rich, N.B., Howard, R.A.: 2004, *J. Geophys. Res.* **109**, A07105. DOI.
Zurbuchen, T.H., Richardson, I.G.: 2006, *Space Sci. Rev.* **123**, 31. DOI.